Marine Geology 380 (2016) 205–218

Contents lists available at ScienceDirect

Marine Geology

journal homepage: www.elsevier.com/locate/margo

Evaluating deep subsidence in a rapidly-accreting mangrove forest using GPS monitoring of surface-elevation benchmarks and sedimentary records

Andrew Swales [a,d,*], Paul Denys [b], Vernon I. Pickett [c], Catherine E. Lovelock [d]

[a] National Institute of Water and Atmospheric Research, Hamilton, New Zealand
[b] School of Surveying, University of Otago, Dunedin, New Zealand
[c] Science and Strategy Directorate, Waikato Regional Council, Hamilton, New Zealand
[d] The School of Biological Sciences, The University of Queensland, St Lucia, Queensland, Australia

ARTICLE INFO

Article history:
Received 3 August 2015
Received in revised form 17 April 2016
Accepted 20 April 2016
Available online 22 April 2016

Keywords:
Radioisotopes
Relative sea-level rise
Accommodation space

ABSTRACT

Ultimately, the fate of mangrove forests depends on substrate-elevation gains keeping pace with relative sea-level rise (RSLR). Some of the world's largest mangrove forests occur on tectonically active margins, river deltas and sedimentary basins where sea-level trends are largely controlled by vertical land motion (i.e., subsidence), so that RSLR can be markedly higher than sea-level rise induced by climate warming. The Rod Surface Elevation Table — Marker Horizon (RSET-MH) method has been applied globally to evaluate coastal-wetland resilience to SLR by quantifying net rates of elevation change relative to a benchmark. A limitation of the RSET method is that the stability of the benchmark (i.e., vertical trend) is unknown and RSLR in wetlands is typically inferred from regional tide-gauge records. In the present study, we evaluate RSLR in a rapidly-subsiding *Avicenna marina* mangrove forest with a large terrigenous sediment supply (Firth of Thames, New Zealand) using independent and complimentary methods: (1) campaign-GPS surveys of the stability of three RSET benchmarks driven 18 m into unconsolidated sediment, a tide gauge some 10 km distant and a reference station located on basement rock (2007–2016) that are tied to a network of satellite-based geodetic sites; and (2) ^{137}Cs-validated ^{210}Pb sediment accumulation rates (SAR) measured in cores as a proxy for RSLR. The similarity of deep-subsidence rates at the RSET benchmarks located several-hundred metres apart (7.7 ± 0.5 to 9.4 ± 0.5 mm yr^{-1}) provides confidence in these results. These subsidence rates are two- to five-fold higher than recorded at the nearby tide gauge (3.6 ± 0.7 mm yr^{-1}) and reference station (1.6 ± 0.5 mm yr^{-1}). Weighted-average ^{210}Pb SAR of 9.9 mm and 9.3 mm yr^{-1} yield similar estimates of deep subsidence (i.e., 8.4 and 6.9 mm yr^{-1} + SLR adjusted for vertical land motion), indicating that this geological process is the major driver of the long-term sea-level trend in the mangrove forest. Our findings suggest that regional tide gauge records may not provide reliable estimates of RSLR for all coastal wetlands due to local subsidence associated with natural processes and human activities. Subsidence rates and RSLR within coastal wetlands can be evaluated using campaign-GPS surveys of RSET benchmarks and independently from longer-term sedimentary records. Finally, evaluations of the resilience of coastal wetlands to rising sea levels over the coming decades must be based on measurements of RSLR from these systems themselves.

1. Introduction

Mangrove forests and salt marshes occupy a narrow elevation window in the intertidal zone above mean sea level (MSL) (Galloway, 1982; Bird, 1986; Ellison, 1993). This lower-elevation threshold for mangrove establishment on tidal flats primarily relates to the physiological tolerance of seedlings of low oxygen concentrations during emersion (i.e., oxygenation of tissues, Clarke and Hannon, 1970; Curran et al., 1986; Hovenden et al., 1995). Consequently, local surface elevation relative to sea level exerts a first-order control on mangrove-forest ecology.

Because mangrove forests are confined to their position within the upper half of the intertidal zone they are sensitive to changing sea level and sediment supply (Cahoon et al., 2006; McKee et al., 2007; Alongi, 2008; Woodroffe and Davies, 2009; Krauss et al., 2013). Ultimately, the long-term fate of a mangrove forest depends on substrate-surface elevation increasing at a rate at least equal to the local rate (i.e., relative) of sea-level rise (RSLR), where vertical land motion (VLM, i.e., uplift, subsidence) interacts with sea-level fluctuations associated with climate change and variability (Nerem et al., 1998; Church and White, 2011; Santamaría-Gómez et al., 2012;

* Corresponding author at: NIWA, P.O. Box 11-115, Hamilton 3251, New Zealand.
E-mail address: Andrew.Swales@niwa.co.nz (A. Swales).

http://dx.doi.org/10.1016/j.margeo.2016.04.015
0025-3227/

Wöppelmann et al., 2014; Watson et al., 2015). Early-Holocene mangrove forests were inundated by rapidly rising sea levels (5–15 mm yr^{-1}), with evidence of these former forests preserved in continental-shelf sediments (Woodroffe, 1992; Ellison, 2008; Woodroffe and Davies, 2009). Modern mangrove forests have, in general, adapted to rates of SLR of up to 5 mm yr^{-1} over the last century (McKee et al., 2007; Cazenave and Llovel, 2010; Church and White, 2011; IPCC, 2013) through vertical accretion of mineral and/or organic sediments. In the present study, we use the independent and complementary methods of campaign-GPS monitoring of benchmarks and estimates of sediment accumulation rates (SAR) derived from cores to quantify the relative contributions of subsidence associated with regional tectonic and local sedimentary processes to RSLR in a mature coastal wetland.

At a global scale, information on the response of contemporary mangrove-forests and salt marshes to rising sea level is sparse (Webb et al., 2013). Increases in global mean sea level (GMSL) are predicted to reach 8–16 mm yr^{-1} by 2081–2100 AD under likely green-house gas emission scenarios (IPCC, 2013). Local environmental conditions controlling rates of RSLR will play a large role in determining the fate of coastal wetlands. Sediment supply via peat production, in autochthonous systems, and mineral-sediment yields from watersheds are influenced by climate variability. Human activities associated with land use and river engineering has also greatly modified sediment yields delivered to coastal environments. In many regions, reductions in sediment delivery are associated with construction of dams as well as improved land management (Walling, 1999; Syvitski et al., 2005). Expansion of coastal wetlands over the last several-hundred years is also a legacy of historical pulses of sediment delivery associated with large-scale catchment deforestation (Morrisey et al., 2010; Weston, 2014). Long-term sea-level trends and shorter-term cycles (e.g., Inter-decadal Pacific Oscillation, ENSO, Rogers et al., 2013; Lovelock et al., 2015b) as well as oceanographic processes (e.g., storm surge, Cahoon, 2006) also influence sediment delivery to mangrove forests by elevating sea level over a range of time scales.

In some settings, sea-level trends are largely controlled by VLM, so that RSLR differs markedly from global and regional patterns of sea-level change (Alongi, 2008; Meckel, 2008; Day et al., 2011; Slangen et al., 2014; Watson et al., 2015). Key drivers of VLM, operating over a range of temporal–spatial scales, include Glacial Isostatic Adjustment (GIA), tectonic processes at active margins (i.e., coseismic, post-seismic and interseismic subsidence) and compaction of unconsolidated sediments (e.g., Törnqvist et al., 2008). Natural sediment compaction in basins and on rapidly accreting river deltas can be exacerbated by reduced sediment supply, fluid extraction (i.e., water, hydrocarbons) and reduced groundwater recharge during droughts (e.g., Carminati and Martinelli, 2002; Peltier, 2004; Phien-wej et al., 2006; Syvitski et al., 2009; Day et al., 2011; Brown and Nicholls, 2015).

Cahoon and Guntenspergen (2010) have defined the resilience of coastal wetlands to sea-level rise in terms of "elevation capital", being the elevation of a wetland relative to the lowest viable elevation in its growth range. Coastal wetlands located in the upper intertidal zone of a macrotidal estuary, for example, will therefore have a much larger potential growth range and elevation capital and consequently will have a greater capacity to maintain surface elevation relative to sea-level than a wetland in a microtidal estuary all other factors being equal. Maintenance of this elevation capital over the long-term largely depends on sufficient deposition of mineral sediments supplied by rivers, in situ production of organic sediments and root growth (Krauss et al., 2003; McKee et al., 2007; Lovelock et al., 2011; McKee, 2011; Krauss et al., 2013; Swales et al., 2015), with the relative contribution of these biophysical processes being site dependent. In turn, RSLR largely depends on the geological processes and/or human activities controlling the subsidence of deltas and sedimentary basins. These large-scale geological processes controlling vertical land motion can rapidly reduce the elevation capital of coastal wetlands (Reed, 2002) unless matched by sediment supply and/or biological processing driving surface-elevation gain.

Assessments of coastal wetland resilience to rising sea level depend on quantifying the net rate of surface-elevation change relative to a local vertical datum. Vertical rates of sediment accretion, determined from buried plates or artificial marker horizons laid on the substrate, typically over estimate net surface-elevation gain. This is because these methods do not integrate the effects of shallow subsidence associated with sediment dewatering and compaction, particularly in organic-rich sediments (Kaye and Barghoorn, 1964; Cahoon et al., 1995, 1999; Cahoon, 2014). The Surface-Elevation Table — Marker Horizon (SET-MH) method has been widely applied to studies of mangrove-forest and salt marsh ecosystems to address a range of research questions, including their response to sea-level change (e.g., Boumans and Day, 1993; Cahoon et al., 1995; Webb et al., 2013; Krauss et al., 2013). Surface-elevation changes can be measured to a high degree of accuracy and are defined relative to a sub-surface datum, usually the base of the SET benchmark. The SET literature recognises that surface-elevation changes in coastal wetlands integrate deep subsidence, shallow subsurface and surface biophysical processes. Key processes include net below-ground biomass production, mineral sedimentation and compaction processes associated with de-watering of recent deposits (i.e., shallow subsidence, S_S), as well as deep subsidence (S_D) due to large-scale geological processes, as described above. In practice, S_S is measured above the SET subsurface datum, whereas S_D is defined as elevation loss below the subsurface datum and is not captured by the SET measurements.

A limitation of coastal-wetland vulnerability assessments incorporating SET measurements is that the stability (i.e., vertical motion) of the SET benchmark is unknown. Typically, SET benchmarks are also not routinely levelled to a local vertical datum so that the elevation capital of a coastal wetland, in terms of its present position in the tidal frame is unknown (Webb et al., 2013). Furthermore, rates of RSLR within a coastal wetland are commonly inferred from regional tide-gauge records and/or geodetic surveys of benchmarks on land rather than directly measured in coastal wetlands themselves (e.g., Rogers et al., 2005; Meckel, 2008; Kolker et al., 2011; Lovelock et al., 2011). Spatial variations in vertical land motion imply that RSLR estimates from tide gauges may not be representative of sea-level changes experienced locally in coastal wetlands (Fadil et al., 2013; Cahoon, 2014).

Recent advances in land-survey technology, in particular the establishment of continuous Global Positioning System (cGPS) networks are now routinely used to monitor land motion, both horizontal and vertical, and have been used to isolate sea-level trends associated with climate change from long-term tide-gauge records of RSLR (Santamaría-Gómez et al., 2012; Fadil et al., 2013; Wöppelmann et al., 2014; Watson et al., 2015). Estimating reliable precision estimates in GPS time series is a critical but challenging aspect of interpreting geophysical signals. Previous studies (e.g. Mao et al., 1999; Williams et al., 2004; Beavan, 2005; Hackl et al., 2011), suggest that cGPS time series consists of "coloured noise" that includes random walk, flicker noise and white noise that is a result of benchmark stability as well as regional scale atmospheric or hydrological mass redistribution errors. Multi-year GPS time series, collected using survey-grade receivers and advanced data analysis, suggest that the velocity precision should be ± 0.5 mm yr^{-1} (e.g. Blewitt and Lavallée, 2002; Wallace et al., 2004; Beavan et al., 2010). To eliminate velocity bias due to the effect of seasonal signals, Blewitt and Lavallée (2002) recommended that data span a minimum of 4.5 years. Thus, GPS technology can be applied to directly monitor the vertical motion of SET benchmarks over multiple years and thereby quantify deep subsidence and the actual trajectory of coastal wetlands relative to sea level.

Surface-elevation records from SET stations are relatively short (i.e., <20 years; Cahoon, 2014) in comparison to many tide-gauge records. Monitoring of benchmarks using GPS survey methods, even over several years, may not be long enough to detect a trend if

subsidence rates are low (e.g., Doyle et al., 2010). Sedimentary records preserved in coastal wetlands can provide alternative reliable long-term proxies for RSLR that incorporate vertical land motion and are consistent with 20th century tide-gauge records (e.g., Gehrels et al., 2002, 2008). In mature coastal wetland systems growing near the upper limit of the tidal frame in sediment-rich settings, net sediment accumulation rates (SAR) measured in cores can provide a proxy for RSLR. In these mature systems, sediment delivery is limited to extreme high tides so that additional (vertical) sediment accommodation space is created by increases in relative sea level (Jervey, 1988; Posamentier et al., 1988; Schlager, 1993; Soreghan and Dickinson, 1994; Gehrels et al., 2008). Mangrove forests and salt marshes are also characteristically sediment sinks (i.e., minimal resuspension) so that long-term SAR will ultimately approach RSLR.

In the present study, we evaluate the use of independent and complementary methods not previously used in combination (i.e., campaign-GPS monitoring of SET benchmark and tide-gauge stability as well as sediment accumulation rates measured in dated cores) to determine subsidence rates in a rapidly-accreting mangrove forest. In particular, we test if GPS measurements of subsidence, in combination with sedimentary records, can be used to quantify the relative contributions of subsidence associated with regional tectonic and local sedimentary processes (e.g., compaction) to RSLR in a mature coastal wetland over multi-year time scales. The geomorphic evolution of the mangrove forest is interpreted within the conceptual framework of sequence stratigraphy and the influence of sea-level and sediment supply on accommodation space (e.g., Jervey, 1988; Posamentier et al., 1988; Schlager, 1993) in coastal wetlands. We present a method to evaluate coastal-wetland resilience to sea-level rise based on surface-elevation trends from RSET and in situ measurements of RSLR.

2. Regional setting

The Firth of Thames is a large (i.e., ~800 km^2) mesotidal estuary located on the northeast coast of New Zealand's North Island (37.21°S 175.45°E, Fig. 1). The North Island is located on the eastern margin of

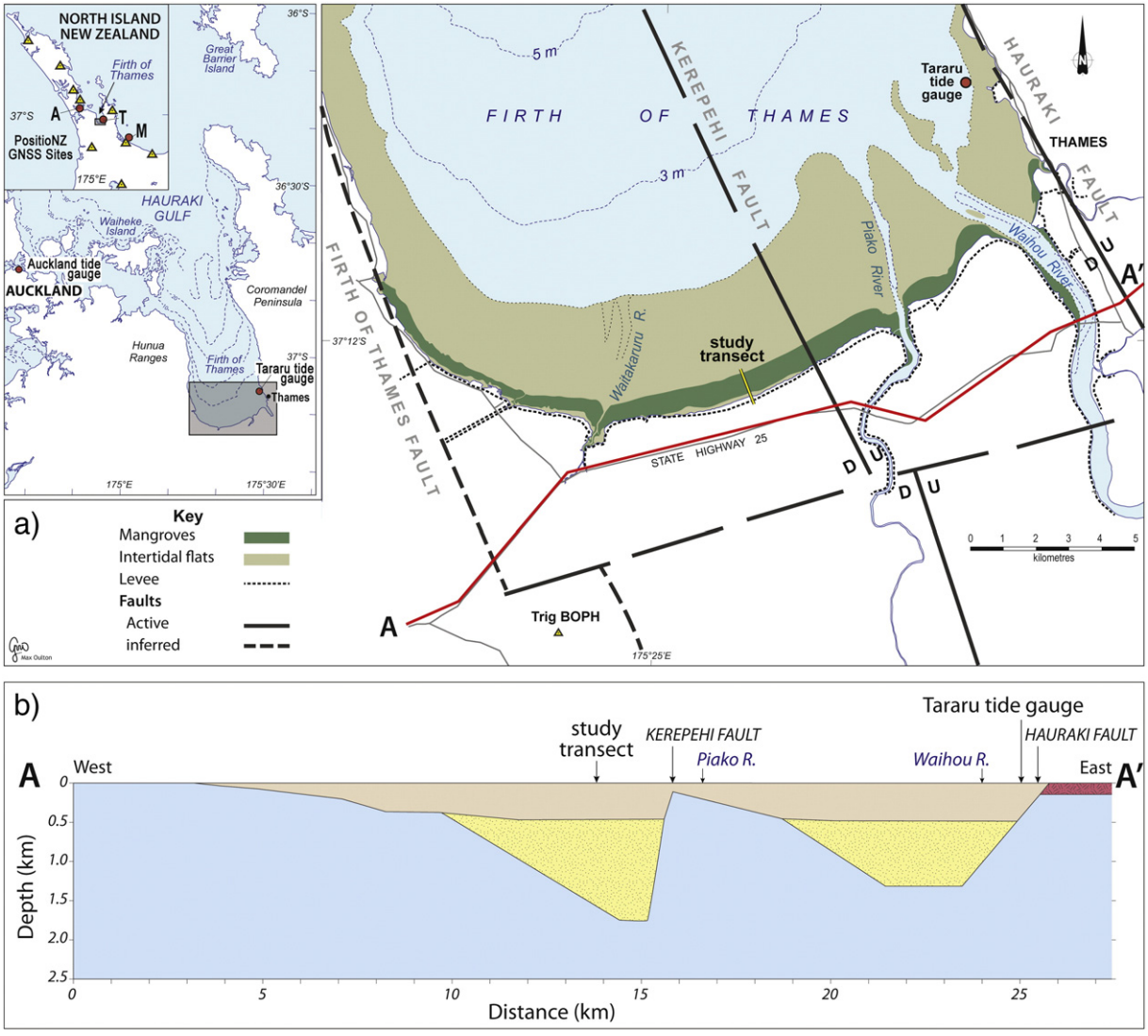

Fig. 1. (a) Location of the Firth of Thames study site, east coast of New Zealand's North Island. Study transect for Rod Surface Elevation Table (RSET) and sediment core measurements shown, with location of the GPS reference station (Trig B0PH) and the Tararu tide gauge. Orientation of normal faults within the Hauraki Rift, with their upthrust (U) and downthrust (D) sides indicated. Locations of: (1) Land Information New Zealand PositioNZ Global Navigation Satellite System (GNSS) geodetic sites used to process GPS measurements from the present study; and (2) the Auckland (A), Tararu (T) and Moturiki (M) tide gauges are shown in the inset map; (b) geological cross-section for transect A-A′ inferred from gravity and magnetic measurements. Major stratigraphic units identified are: Greywacke basement (blue); Tertiary sediments (yellow); Quaternary sediments (light brown); and Tertiary volcanic rocks (red). Approximate locations of study transect and the Tararu tide gauge is also shown. Fig. 1b reproduced and modified from Hochstein, M.P. and Nixon, I.M. (1979). New Zealand Journal of Geology and Geophysics 22(1), 1–19 with permission of Taylor and Francis Ltd., www.tandfonline.com.

the Australian Plate, under which the Pacific Plate is subducting (Pillans, 1986). The Firth occupies part of the tectonically-active Hauraki Rift, an ~25 km wide and ~250 km long rift-valley system (Hochstein and Nixon, 1979; Hochstein et al., 1986). Geophysical surveys of the rift section beneath the southern Firth of Thames and Hauraki Plains, immediately to the south, indicate the presence of three roughly parallel NNW-striking normal faults. The faults dip steeply west (~70°), forming deep sedimentary basins beneath the Firth that have infilled with Tertiary–Quaternary sediments to a maximum depth of about 3 km (Hochstein and Nixon, 1979). Unconsolidated Quaternary sediments extend to 0.7–1 km depth, suggesting subsidence in these basins (Hochstein et al., 1986; Pillans, 1986).

The Kerepehi Fault, near the centre of the rift, forms the boundary between the sedimentary basins to the east and west of the fault. Greywacke basement rock comes within 100 m of the land surface immediately east of the fault near the Piako River (Hochstein and Nixon, 1979). The measurement transect in the present study is located within the western basin approximately 2 km west of the Kerepehi Fault (Fig. 1). Further north, the fault is interrupted by three roughly west–east trending transverse faults (Chick et al., 2001). The Kerepehi Fault is active, as indicated by shallow seismic activity and hot springs (Hochstein and Nixon, 1979).

De Lange and Lowe (1990) reconstructed the magnitude and frequency of vertical displacement of the Kerepehi Fault (south of the Firth) associated with several large earthquakes during the Holocene using dated tephra layers preserved in freshwater-marsh sediments. Cumulative vertical displacement of the fault by an estimated 1.6 m has occurred during four seismic events (range: 0.2–0.7 m per event), having an average recurrence interval of ~2500 years. Within the southern Firth itself, geophysical data from marine sediments suggest vertical displacement of at least 4 m on the Kerepehi Fault over the last 6500 years (Chick et al., 2001).

Interseismic subsidence rates for the Hauraki Rift sedimentary basins associated with regional tectonism and/or compaction are presently undetermined. Studies in other basins with kilometres-thick sedimentary sequences, such as the Mississippi, indicate that decadal-to-centennial subsidence rates can average several millimetres or more per annum largely due to natural sediment compaction and/or fluid extraction (e.g., Meckel, 2008; Törnqvist et al., 2008; Kolker et al., 2011).

Major sources of terrigenous sediment accumulating in the southern Firth are the Waihou (1966 km^2) and Piako (1476 km^2) Rivers (Fig. 1), which account for ~96% of the 3600 km^2 land catchment. These rivers presently deliver an estimated 160,000 t yr^{-1} and 30,000 t yr^{-1} respectively of suspended sediments to the southern Firth (Hicks et al., 2011). Peak sediment influxes to the Firth coincided with large-scale catchment deforestation during the mid-late 1800s associated with timber extraction, gold mining and land conversion to pastoral agriculture by European settlers (Healy, 2002; Swales et al., 2015).

The Firth of Thames progressively shoals from north (35 m depth) to south. Tides are semi-diurnal, with average spring- and neap-tidal ranges of 2.9 m and 2.2 m, respectively. Prevailing and opposing southwest–northeast winds drive clockwise and anticlockwise residual circulation that traps river-borne suspended sediments within the southern Firth (Healy, 2002). The combination of a relatively large tidal range and sediment supply, as well as physical processes that favour sedimentation has built ~70 km^2 of intertidal mudflats in the southern Firth (Fig. 1).

The Port of Auckland (located 74 km northwest of the study site, Fig. 1) has the nearest tide gauge with a long-term record and shows a RSLR of 1.5 ± 0.1 mm yr^{-1} (1899–2008 A.D., Hannah and Bell, 2012), which is similar to the rate of increase in Global Mean Sea Level (GMSL) of 1.7 mm yr^{-1} (range: 1.5–1.9 mm yr^{-1}) between 1901 and 2010 (IPCC, 2013). An updated rate for long-term RSLR at Auckland, including the period 2009–2015 is 1.6 ± 0.08 mm yr^{-1} (Fig. 2). During the satellite altimetry era (1993–2015), RSLR at Auckland has averaged

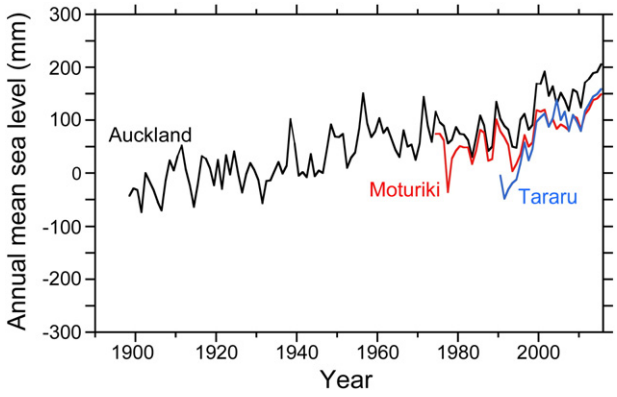

Fig. 2. Annual mean sea level time series for tide gauges at Auckland (1899–2015), Moturiki (Bay of Plenty, 1974–2015) and Tararu (Firth of Thames, 1993–2015). Locations of tide gauges are shown in Fig. 1. Data sources: Ports of Auckland, NIWA and Waikato Regional Council.

4.9 mm yr^{-1} (Supplementary Information A) in comparison to the GMSL rate of 3.3 mm yr^{-1} (https://www.cmar.csiro.au/sealevel/). A short tide record for the southern Firth at Tararu (Figs. 1, 2), coinciding with the satellite era, indicates a RSLR of 6 mm yr^{-1} (1993–2015). The Moturiki tide gauge, located 83 km south-east of the study area in the Bay of Plenty, has recorded a RSLR of 2.3 mm yr^{-1} (1974–2015) in comparison to 3.0 mm yr^{-1} at Auckland (Fig. 2, Supplementary Information A).

Mangrove forest (*Avicennia marina* var. *australasica*) has colonised ~11 km^2 of the upper intertidal flats in the southern Firth since the early 1960s (Swales et al., 2015), which occur close to the southernmost limit of mangroves globally (i.e., 38.9°S, Corner Inlet, South Victoria, Australia (Bird, 1986)). The mangrove forest occupies an ~800 m wide platform at supratidal elevations (i.e., 1.7–1.9 m MSL), with hydroperiod (i.e., frequency and duration of submergence) being less than 3% (Swales et al., 2015). Mangrove-forest development is a recent phenomenon with mangrove trees restricted to river deltas until as recently as the early 1950s. The mangrove forest has accumulated up to two metres of uniformly fine-grained muds over the last fifty years or so, which have buried a former intertidal sand flat. Swales et al. (2015) recognise several mud facies, indicative of non-vegetated and mangrove-colonised mud flats. These under-consolidated muds have mean and median particle diameters of ~20 μm, with uniformly low dry-bulk sediment densities across the mangrove platform and down core (0.4–0.59 g cm^{-3}, Swales et al., 2015).

3. Materials and methods

Measurements of deep subsidence and sediment accumulation rates were made in the mangrove forest along a shore-normal transect located approximately 2 km west of the Kerepehi Fault and mid-way between the Waitakaruru and Piako River mouths (Fig. 1). Surface elevation was determined along the transect to ± 5-mm accuracy using a Geodimeter 464 total station and reduced to MSL Moturiki Vertical Datum 1953 (MVD-53).

The location of the measurement transect in the southern Firth of Thames was informed by a comprehensive record of historical aerial photography (1944–2005) and earlier work that indicated that the mangrove forest on the upper intertidal flat had rapidly accreted sediment (i.e., up to 100 mm yr^{-1}). Consequently, the oldgrowth mangrove forest (Fig. 3) is now close to the upper limit of the tidal frame and is infrequently inundated (Swales et al., 2015). This indicated that sediment delivery to the old-growth forest, and therefore sediment accumulation rates (SAR), will primarily depend on the creation of sediment accommodation space (Jervey, 1988) by relative sea-level rise. Swales et al. (2015) also showed, by comparison with SET data, that ^{210}Pb SAR is a

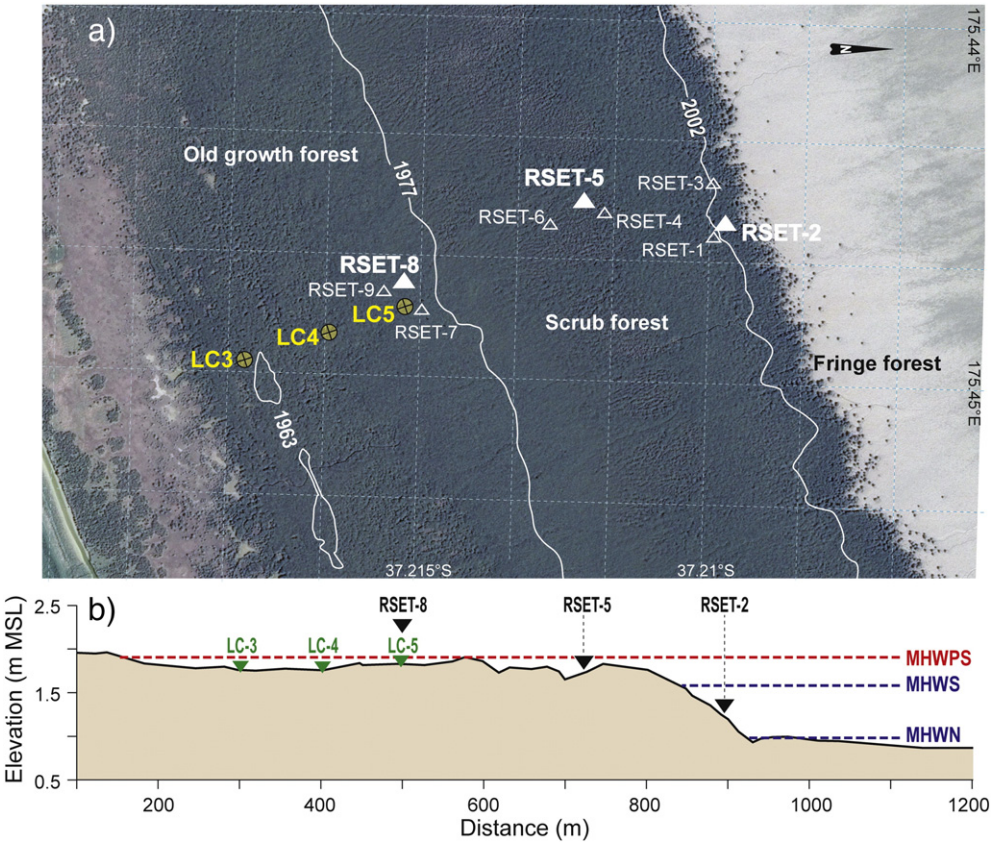

Fig. 3. Mangrove-forest transect: (a) sediment core and Rod Surface Elevation Table (RSET) benchmark locations. Campaign-GPS surveys of the vertical stability of the benchmarks monitored at sites RSET-2, -5 and -8. Historical changes in mangrove-forest extent indicated by white lines; and (b) surface elevation (2005) along a shore-normal profile relative to mean sea level (Moturiki Vertical Datum 1953) with mean high-perigean spring, spring, and neap-tide levels.

reliable proxy for rate of surface-elevation change in the mangrove forest. It follows that SAR in the old-growth forest could provide estimates of deep subsidence rates given a reliable long-term estimate of SLR from a tide gauge adjusted for vertical land motion.

3.1. Surface Elevation Tables

Subsidence rates in the mangrove forest were determined from campaign-GPS surveys of Surface Elevation Table (SET) benchmarks located along the mangrove-forest transect (Fig. 3). The RSET, an improved version of the original SET, is mounted on a stainless-steel rod benchmark driven several to tens of metres vertically into the substrate. The RSET instrument, with an arm which rotates 360° through a level plane, enables high-precision repeat point measurements ($n \leq 72$) of the height of the substrate surface relative to the RSET benchmark (Cahoon et al., 2002).

In the present study, RSET stations were installed during 4–5 February 2007 along the mangrove forest transect. RSET benchmarks, consisting of 12 sections of 1.5 m long threaded and 14.2 mm diameter stainless steel rod were manually driven vertically into the substrate using an ~17.5 kg post-driver with an assisted ~1 m fall. Substantial resistance was met at all sites after 12 sections of rod were inserted (i.e., total of 18 m, Fig. 4). The RSET instrument receivers were bolted to the top of the rod, which extended ~0.6 m above the substrate surface. The installation of the RSET benchmark was completed by encasing the rod and receiver in concrete, to minimise horizontal motion during measurements, by excavating a 0.3 m deep circular pit around the rod and installing a vertical section of 0.15 m diameter by 0.7 m long PVC pipe.

The location of the RSET stations were determined using a stratified-sampling approach, with three stations installed in each of the major forest zones: (a) mature "old-growth" mangrove forest (pre-1980s); (b) scrub forest (mid-1990s–present); and (3) the present-day fringe forest (early 1990s). Campaign-GPS measurements were made over an eight-year period (October 2007 to February 2016) at one RSET station in each of the forest zones: RSET-2, RSET-5 and RSET-8 (Table 1, Fig. 3).

3.2. GPS measurements

The purpose of the campaign-GPS measurements was to confirm the stability, or otherwise, of the RSET benchmarks. In many previous RSET studies of coastal wetlands, the stability of RSET benchmarks is implicitly assumed or subsidence rates are inferred from regional tide-gauge records (e.g., Cahoon, 2014). However, the stability of any RSET benchmark cannot generally be assumed. In the present study, the location of the Firth mangrove forest in an active-rift sedimentary basin suggested that subsidence due to tectonic and/or sediment compaction was likely to be an important driver of RSLR.

Several options for monitoring the height stability of the RSET marks were considered, including terrestrially-based digital levelling as well as high precision total station traverse and space-based positioning using GPS. The terrestrially-based methods were discarded due to the difficulty of working in the mangrove-forest environment. Issues included lack of line of sight, requiring multiple setups due to the density and height of the mangrove trees, poor vertical stability of the setups due to compaction of the soft mud while taking measurements and heat haze, which precluded accurate optical measurements. Methods based on stop-and-go or semi-kinematic GPS, for example real-time kinematic (RTK), post-processed kinematic (PPK), or network RTK, were not considered due to low vertical precision. Typically, height precision is at the $\pm$1–2 cm level (Hofmann-Wellenhof et al., 2001; Edwards et al., 2010).

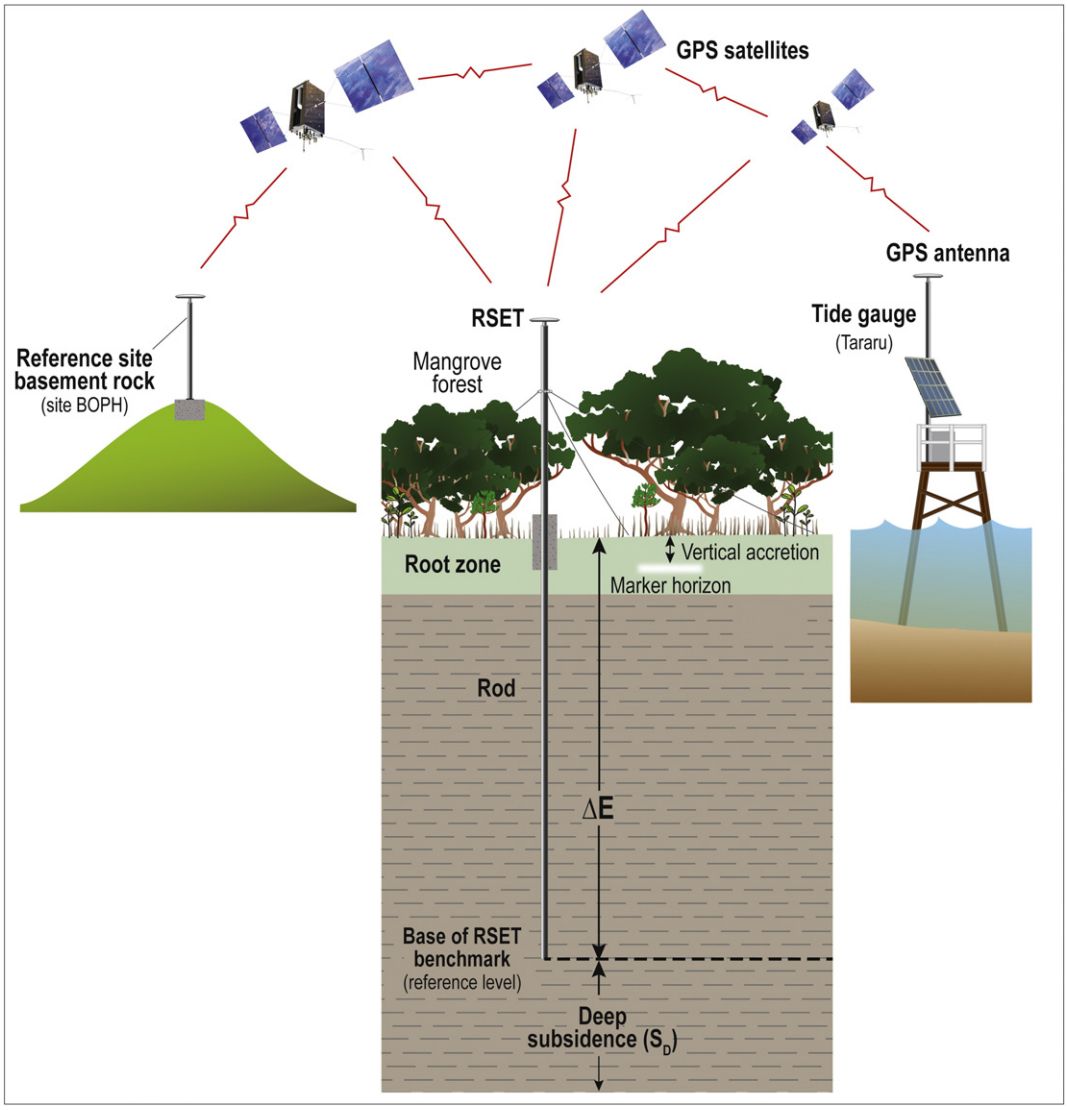

Fig. 4. Campaign-GPS survey definition diagram. Measurements of the vertical stability of Rod Surface Elevation Table (RSET) benchmarks in the mangrove forest, reference station on basement rock (B0PH) and at the Tararu tide gauge. Refer to Fig. 1 for site locations. Deep subsidence (S_D) and change in surface elevation (ΔE) are defined relative to the base of the RSET benchmark. The surface-elevation trend relative to the RSET benchmark does not account for S_D.

For these reasons, repeat surveys using static GPS of the RSET benchmarks was considered the most reliable and accurate technology in this environment (Soler et al., 2006; Häkli et al., 2008; Firuzabadi and King, 2012; Kearns et al., 2015). The establishment of long-term continuous GPS at sites within the mangrove forest, requiring additional well-established survey marks and continuous power supply (e.g., photovoltaic panels), was not feasible with the available resources.

Table 1
Summary of campaign-GPS measurements, Firth of Thames.

Campaign	Dates	Duration (days)
1	16–24 October 2007	9
2	17–20 April 2008	4
3	27–30 June 2008	4
4	15–23 October 2008	9
5	16 Nov.–1 Dec. 2009	6
6	2–8 November 2010	7
7	19–24 January 2012	6
8	13–19 December 2012	7
9	8–13 January 2014	6
10	25–29 February 2016	5

High-precision campaign-GPS uses geodetic or survey grade receivers operated over multiple days. The receivers are set to log carrier phase data (30 s epoch intervals) and typically track between 8 and 12 GPS satellites. The antenna is erected above the reference mark (survey benchmark) using a fixed length carbon-fibre antenna pole to reduce antenna height variations due to temperature. A pole was constructed for each location with known heights of between 0.3 and 3.2 m and fixed in place vertically using four guy-ropes anchored by the trunks of mangrove trees and spaced equally at ~90° angles. To minimise positioning errors, all stations are occupied at the same time ensuring that the receivers are logging data simultaneously. Multi-day data acquisition helps to minimise small but significant night/day biases and improves modelling of the atmospheric conditions.

Monitoring of survey/benchmarks requires control or reference marks that are assumed to be stable relative to the monitoring marks (i.e. benchmarks). In many environments, and especially in coastal wetlands, control mark stability is not known or cannot be guaranteed. This is also the case in many parts of New Zealand as the country straddles the Pacific–Australian tectonic plates and the Firth of Thames is located within the active Hauraki Rift zone. In addition to the RSET campaign-GPS data, over 20 continuous Global Navigation Satellite System (cGNSS) stations in the Land Information New Zealand (LINZ) PositioNZ

network (apps.linz.govt.nz/positionz) were included (Supplementary Information A, B). Combining the campaign data with the cGNSS sites provides a connection to other survey marks that have been reliably established, have a long history and are continuously monitored.

The height or vertical component of land motion is particularly difficult to measure. Results from continuous GPS sites based on 24 h data sets, indicate horizontal root-mean-square (rms) values typically of ±1–2 mm, while the vertical component is often 3–4 times less precise with rms values of ±4–6 mm (Cenni et al., 2013; Pearson et al., 2015). The reason for this is that GPS systematic biases have a greater effect on the vertical component. These biases include atmospheric delays (ionosphere, troposphere), multipath, antenna phase centre, antenna height measurement and the GPS constellation. To mitigate the effects of these factors, various field methods and techniques were adopted, which include: (1) The same receiver and antenna type have been used for all surveys (Supplementary Information A); (2) fixed-length antenna poles. Carbon-fibre antenna pole of known length were used at each GPS measurement station, with the same pole used at each station to eliminate antenna-height measurement errors. Pole lengths of 0.3 to 3.2 m were required to elevate the GPS antenna above the mangrove-forest canopy. The lengths of the poles were kept as short as possible to ensure a stable antenna setup during the measurement campaign; (3) Long observing periods. Data were logged for nominally 24 h sessions over 3–4 days, as dictated by the battery life. These extended observation periods allow for better characterisation of the troposphere component of the atmosphere; (4) Dual frequency receivers, which allow for the mitigation of the ionosphere delay; (5) Antenna Phase Centre corrections based on internationally accepted calibrated antenna models; and (6) Geodetic-quality antenna with ground planes to reduce the effects of errors caused by signal multipath.

The GPS data were collected at a single station within each of the three RSET clusters (i.e., RSET-2, RSET-5, RSET-8, Fig. 3). In addition to the RSET benchmarks, an additional reference site was established (RSET-0) 9 km south-west of the mangrove-forest transect (Trig B0PH, Fig. 1). From a geological perspective, this hill-top site should be stable as it is located on the underlying greywacke rocks of the Mesozoic Waipapa terrane that forms part of the uplifted "horst" rather than the Hauraki Graben (Hochstein and Nixon, 1979). The stability of the Tararu tide gauge (TARU), located 11.4 km north-east of the transect was also measured by campaign-GPS measurement (Fig. 1, Supplementary Information C). The GPS antenna, attached to a one-metre long carbon-fibre pole, was mounted on a threaded bolt permanently fixed to the ~2 × 2 m wooden deck of the tide gauge platform and attached to the same structure as the tide gauge housing.

In total, ten GPS campaigns were conducted, with the first measurements collected in October 2007, nine months after installation of the RSET benchmarks (Table 1). The RSET stations were initially occupied at approximately three-month intervals during the first 12 months to provide a reference (i.e., October 2007, April, June and October 2008), and subsequently at annual intervals until January 2014. The last survey was conducted in February 2016. Table 2 provides details of the locations of the RSET benchmarks, RSET-0 reference station and the Tararu tide gauge.

The GPS carrier-phase data were analysed using the Bernese v5.2 software (Dach et al., 2015) to determine daily (i.e., 24 h) estimates of the relative coordinates. High-precision models and GNSS products were used, including precise orbits and satellite clocks (CODE), and corrections applied for the antenna-phase centre (IGS), the FES2004 ocean-tidal loading model and atmospheric tidal-loading model (see also Supplementary Information A).

The combined daily network is processed in terms of ITRF2008 (Altamimi et al., 2012), accounting for offsets caused by equipment changes (i.e., antenna offsets), earthquake co-seismic events, East Coast slow slip events and other transient land motions. Each GPS campaign was combined into a single solution. Data outliers are removed at the 4σ level, where σ is estimated using the Median Absolute Deviation (MAD) robust estimator with $\sigma = 1.4826 \times \mathrm{MAD}$. No seasonal terms (annual/semi-annual trends) were estimated due to the limited nature of the data. The horizontal components (i.e., northing and easting) of land motions at the mangrove-forest RSETs, Tararu and RSET-0 reference stations were also determined relative to the Auckland LINZ PositioNZ GNSS site (AUCK, Supplementary Information B). This comparison quantifies the horizontal motion of the stations relative to the Australian tectonic plate.

3.3. Sedimentary record–accumulation rates

Sediment accumulation rates (SAR) in the pre-1980s "old-growth" mangrove forest were determined at three core sites based on excess lead-210 ($^{210}Pb_{xs}$) and caesium-137 (^{137}Cs) activity profiles (Fig. 3). Duplicate sediment cores up to 2 m long and 7.5 cm diameter were collected in February 2005 at sites LC-3, LC-4 and LC-5 using a Livingstone piston-corer.

Methods for estimation of apparent SAR from analysis of $^{210}Pb_{xs}$ and ^{137}Cs profiles preserved in the cores are described in detail by Swales et al. (2015) and summarised here. Activities of total ^{210}Pb (46.5 KeV peak), ^{137}Cs (661 KeV) and ^{7}Be (477 KeV) were determined by gamma-spectrometric analysis using standard methods. Dried and ground sediment sub-sampled (50–60 g) at down-core intervals were embedded in resin to allow ingrowth of ^{210}Pb parent radioisotopes for 30 days prior to counting. Excess ^{210}Pb activity was determined by subtracting supported ^{210}Pb activity, due to the decay of radium-226 (^{226}Ra, $t_{1/2}$ 1600 yr), from total ^{210}Pb activity and decay corrected for the elapsed time since sample collection. Radioisotope activities are reported in S.I. units of Becquerels per kilogram (Bq kg^{-1}). Uncertainty in $^{210}Pb_{xs}$ activity at the 95% confidence level was calculated using standard methods (Joint Committee for Guides in Metrology, 2008.

Time-average SAR were estimated from $^{210}Pb_{xs}$ profiles assuming that accumulation rather than mixing is the dominant process below the surface mixed layer (SML) and steady-state conditions exist (Krishnaswami et al., 1980; Nittrouer and Sternberg, 1981) so that sediment accumulation rate (S, mm y^{-1}) can be estimated by a least-squares fit to:

$$A_z = A_0 \exp.(-\lambda z/S) \quad (1)$$

where A_z is the excess ^{210}Pb activity at depth z, λ is the decay constant for ^{210}Pb (i.e., 0.0311^{-1} year), and A_0 = excess ^{210}Pb activity at the top of the core interval. The apparent age of sediment at a particular depth is therefore an exponential function of A_0 and S. The depth of the ^{7}Be SML, was typically less than 2 cm in the mangrove forest (Swales et al., 2015). The ^{210}Pb SAR were validated using the maximum

Table 2
Location of RSET Benchmarks, RSET-0 reference site and Tararu tide gauge, Firth of Thames. NZGD2000 Geodetic and New Zealand Transverse Mercator (NZTM-2000) coordinates.

Station	Latitude (South)	Longitude (East)	NZTM Easting (m)	NZTM Northing (m)
RSET-2	−37° 12′ 27.00″S	175° 26′ 45.58″S	1,817,060	5,879,306
RSET-5	−37° 12′ 32.88″S	175° 26′ 45.24″S	1,817,047	5,879,125
RSET-8	−37° 12′ 39.26″S	175° 26′ 45.56″S	1,817,148	5,878,925
RSET-0	−37° 16′ 40.82″S	175° 23′ 09.64″S	1,811,539	5,871,618
Tararu	−37° 07′ 40.56″S	175° 31′ 17.80″S	1,824,006	5,887,959

penetration depth of ^{137}Cs in the sediment cores, with atmospheric deposition of ^{137}Cs in New Zealand first detected in 1953 (Matthews, 1989). For ^{137}Cs sediment dating, we assume that: (1) ^{137}Cs was rapidly transferred to depositing sediments after initial introduction and reached peak activities in 1963; (2) ^{137}Cs was rapidly mixed into sediment upon delivery by biophysical processes; and (3) core compaction is minimal, as indicated by dry-bulk sediment density profiles (Swales et al., 2015), so that the ^{137}Cs accumulation rate, S, can be calculated from:

$$S = (z_p - z_b)/(t_0 - t_i) \quad (2)$$

where z_p = the maximum penetration depth of ^{137}Cs (cm), z_b = depth of rapid mixing (cm), t_0 = year sediment core collected (i.e., 2005) and t_i = the year ^{137}Cs was first introduced to the environment (Swales et al., 2015).

4. Results

4.1. Subsidence

The vertical trend estimated for each of the three RSET benchmarks, RSET-0 reference site and the Tararu tide gauge (TARU) are presented in Table 3 and Fig. 5. These data indicate that the RSET benchmarks located in the mangrove forest are subsiding rapidly relative to sea level measured at Auckland. Subsidence rates at the mangrove forest benchmarks vary from 7.7 to 9.4 mm yr^{-1}, which are statistically significant ($r^2 \geq 0.97$, $P < 0.001$). The Tararu tide gauge is also subsiding at 3.6 mm yr^{-1} ($r^2 = 0.74$, $P < 0.01$) albeit less rapidly than the RSET benchmarks. The reference benchmark RSET-0, located on underlying greywacke bedrock, displays a relatively small subsidence trend of 1.6 mm yr^{-1} ($r^2 = 0.62$, $P < 0.05$). The rms fits of these data to the linear trend is between ±2 and 6 mm and provides a measure of the variability about the straight line trends (Table 3). This variation can often be attributed to limitations in modelling the troposphere bias caused by changeable environmental conditions often found at coastal sites and is typical of what can sometimes be expected from campaign-GPS measurements (Wang et al., 2013; Kearns et al., 2015). By comparison, the mean rms of the vertical trend at PositioNZ sites in the vicinity of the Firth of Thames is ±4.7 mm, for data periods exceeding 15 years.

The analysis also shows that rates of horizontal land motion at the mangrove-forest RSET benchmarks, Tararu tide gauge and RSET-0 reference stations, the LINZ PositioNZ stations north of Hamilton (Fig. 1), and GPS data (1995–2013) used to determine the National velocity field (Beavan et al., 2016), are negligible relative to the Auckland LINZ PositioNZ station. This apparent lack of relative horizontal land motion at a regional scale suggests that the subsidence observed at the RSET stations and tide gauge is unrelated to rifting in the Hauraki Rift.

4.2. Sediment accumulation rates

Excess ^{210}Pb profiles preserved in cores LC-3 to LC-5 collected from the old-growth mangrove forest indicate several changes in SAR since the 1920s (Fig. 6). The ^{210}Pb geochronology generally shows close agreement with the maximum depth of ^{137}Cs (i.e., post-1953 in New Zealand). These s-shaped ^{210}Pb$_{xs}$ profiles exhibit relatively low SAR near the top (<12 mm yr^{-1}) and bottom (10–22 mm yr^{-1}) of each core. These typically multi-decadal low-SAR periods are separated by a period of rapid sedimentation (33–100 mm yr^{-1}).

The reduction in SAR in the most recently deposited low-SAR layer occurred in the late-1960s to early-1970s at LC-3 and LC-4 and in the early 1990s at LC-5 (Fig. 6b). The regression fits to the ^{210}Pb$_{xs}$ are very good for this recent low-SAR period ($r^2 = 0.79$–0.97). The transition to low SAR from the late 1960s appears to coincide with progressive sedimentation and an increase in surface elevation above mean high water spring (MHWS, 1.6 m MSL) tide level, near the upper limit of the tidal frame.

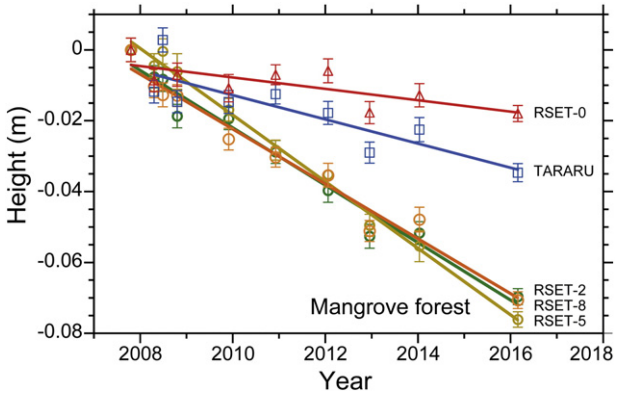

Fig. 5. Firth of Thames RSET benchmarks. Relative vertical trends with linear-regression fits for the mangrove-forest Rod Surface Elevation Tables (RSET-2, -5, -8), reference site RSET-0 and the Tararu tide gauge (October 2007 to February 2016). Precision values are shown as 95% confidence intervals.

Table 3
Firth of Thames RSET benchmark vertical trends (velocity and standard deviation, mm yr^{-1}), number of observations (n) and trend root-mean-square.

Site	$V_h \pm s_h$ (mm yr^{-1})	n	rms (mm)
RSET-0	−1.61 ± 0.48	9	±3.8
TARU	−3.64 ± 0.68	10	±5.7
RSET-2	−8.11 ± 0.47	10	±3.9
RSET-5	−9.40 ± 0.28	10	±2.3
RSET-8	−7.74 ± 0.47	10	±3.9

5. Discussion

5.1. Subsidence, sediment accommodation and sea-level

Campaign-GPS measurements of the RSET benchmarks located across the mangrove-forest platform (2007–2016) indicate that the forest is rapidly subsiding, at a rate averaging 8.8 ± 0.3 mm yr^{-1} (range: 7.7 ± 0.5 to 9.4 ± 0.3 mm yr^{-1}). These vertical trends were determined using weighted least squares regression, with observation weighting based on the velocity standard error. The similarity of the vertical trend measured at the three RSET stations suggests that this subsidence is a relatively uniform process over spatial scales of at least hundreds of metres.

The potential contribution of settlement of the RSET benchmarks to the apparent subsidence trend measured by the campaign-GPS surveys was evaluated using standard geotechnical engineering methods (Supplementary Information A). Specifically, we conservatively estimated the bearing capacity of the benchmark within the unconsolidated sediments (i.e., skin friction resistance) relative to the force exerted by the benchmark mass and the potential point settlement. These calculations indicate that the downward force exerted by the mass of the RSET benchmarks is ~100-times smaller than the bearing capacity. The potential point settlement of the benchmarks in the substrate was also negligible. These calculations suggest that the linear subsidence trend measured by the campaign-GPS surveys is largely due to deep subsidence of the sediment column by compaction and VLM.

Vertical land motion associated with GIA and regional tectonic processes is likely to account for less than 2 mm yr^{-1} of the observed linear trend based on data from RSET-0 and PositioNZ GNSS sites (Supplementary Information A). Contemporary subsidence rates of Mississippi Delta and Gulf of Mexico coastal wetlands of approximately 8 mm yr^{-1}, for example, have been attributed to compaction of near-surface peat deposits (i.e., uppermost ~15 m) and underlying older Holocene mineral

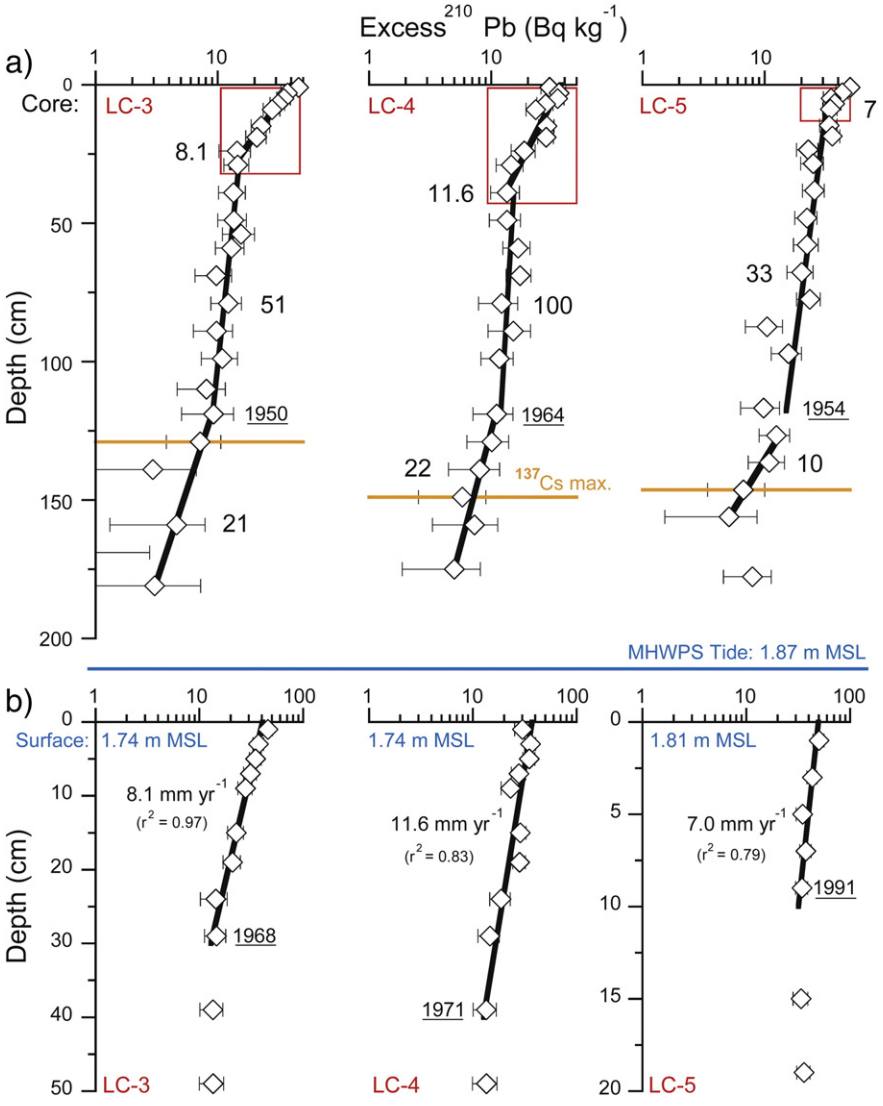

Fig. 6. Old growth mangrove forest (Firth of Thames) excess ^{210}Pb profiles ($^{210}Pb_{xs}$, with 95% confidence intervals) measured in cores LC-3, LC-4 and LC-5. (A) Full $^{210}Pb_{xs}$ profiles with maximum depth of ^{137}Cs-labelled (i.e., post-1953) sediments shown. Regression fits to the $^{210}Pb_{xs}$ data are shown along with time-averaged sediment accumulation rates (mm yr^{-1}); (B) enlargement of the upper $^{210}Pb_{xs}$ profiles, with data and regression fits. Estimated ^{210}Pb-age (underlined) at changes in the profile slope also shown. Substrate surface elevation at time of core collection relative to mean sea level Moturiki Vertical Datum 1953 and Mean High Water Perigean Spring (MHWPS) Tide.

sediments as well as fluid extraction since the 1930s rather than tectonic drivers (Meckel, 2008; Törnqvist et al., 2008; Kolker et al., 2011).

The GPS estimate of total subsidence of the RSET benchmarks (S_T, weighted average 8.8 ± 0.3 mm yr^{-1}, 2007–2016) is within the range of ^{210}Pb SAR in the old-growth forest (7–11.6 mm yr^{-1}) following the transition to a low-SAR regime from the late-1960s. This transition coincides with a large reduction in hydroperiod and associated sediment delivery, following a period of rapid surface-elevation gain (33–100 mm yr^{-1}) on the upper intertidal flat. This rapid aggradation phase began in the 1950s and preceded mangrove colonisation (Swales et al., 2015).

The contribution of total subsidence to RSLR in the mangrove forest is estimated from the ^{210}Pb SAR:

$$S_T = RSLR_{sed} - (RSLR_{tg} + VLM_{tg}) \quad (3)$$

where $RSLR_{sed}$ is the average ^{210}Pb SAR measured in the old-growth mangrove forest, and $RSLR_{tg}$ and VLM_{tg} (−0.6 mm yr^{-1}, Supplementary Information A) are the linear sea level trend and VLM measured at the Auckland tide gauge respectively over the period of sedimentation represented in cores LC-3 to LC-5 (1968/1971/1991 to 2005). The low-SAR regime in cores LC-3 and LC-4 span substantially longer and similar time periods (i.e., 35–38 years) than for LC-5 (i.e., 14 years) so that weighted-average values of $RSLR_{sed}$ and $RSLR_{tg}$ are calculated based on record length. These data yield S_T estimates for the old-growth mangrove forest of 8.4 and 6.9 mm yr^{-1} respectively for the two longest (i.e., LC-3 and LC-4) and all three sediment-core records (Table 4).

Table 4
Total subsidence (S_T) estimated from weighted-mean values of: (1) ^{210}Pb sediment accumulation rates (SAR, mm yr^{-1}) as a proxy for relative sea-level rise ($RSLR_{sed}$, mm yr^{-1}) in the old-growth mangrove forest; and (2) matching sea-level trends at the Auckland tide gauge ($RSLR_{tg}$, mm yr^{-1}). Vertical land motion (VLM) at the tide gauge is approximately −0.6 mm yr^{-1} (Supplementary Info. A).

Core site	Time period (yr)	$RSLR_{sed}$	$RSLR_{tg}$	S_T (mm yr^{-1})
LC-3	37 (*1968–2005*)	8.1	2.15	
LC-4	35 (*1971–2005*)	11.6	1.99	
LC-5	14 (*1991–2005*)	7.0	7.73	
Weighted mean				
LC-3, LC-4	2 cores	9.9	2.1	9.9 − (2.1 + −0.6) = 8.4
LC-, LC-4, LC-5	3 cores	9.3	3.0	9.3 − (3.0 + −0.6) = 6.9

The S_T values estimated from the sedimentary record are similar to the subsidence trend derived from the relatively short-term campaign-GPS measurements of the RSET benchmarks (8.8 ± 0.3–0.5 yr^{-1}). The differences between the ^{210}Pb SAR and GPS-derived estimates have several possible explanations. Firstly, the sediment core records span a longer time period (up until 2005) immediately before the GPS measurements began (2007–2016). This is an unlikely explanation as both sets of measurements can be considered simultaneous relative to the long-term geological processes controlling vertical land motion (i.e., GIA, regional tectonics, sediment compaction). Some of the difference between the S_T estimates may reflect the shorter GPS record and may converge over time as well as uncertainty in the fitted linear trends for the ^{210}Pb SAR and RSET VLM. The S_T core estimates are smaller (by 0.4 and 1.9 mm yr^{-1}) than the GPS-derived value. This may reflect subsurface processes inherent in the sediment core records. These include shallow compaction by dewatering or mangrove leaf litter deposition and decomposition and changes in root biomass/volume in the upper ~0.5 m of the substrate that are not captured by the GPS measurements. Differences due to shallow compaction are, however, limited by the low permeability of these smectite–clay-rich muds (Swales et al., 2015). Lastly, the LC-3/LC-4 S_T estimate is likely to be more representative of conditions in the old-growth forest due to the substantially longer (i.e., two-fold) and multi-decadal record. The delayed transition from a high- to low-SAR regime that occurred at LC-5 in the early 1990s is due to its location on the edge of a former shallow tidal basin that infilled from the mid-1980s onwards (Swales et al., 2015). Although the weighted-average ^{210}Pb SARs for the two-core and three-core cases are similar (i.e., 9.9, 9.3 mm yr^{-1}), the substantially smaller S_T value estimated for the three-core case is exacerbated by the much larger RSLR rate from the Auckland tide gauge for the short LC-5 sedimentation record (i.e., RSLR of 7.7 mm yr^{-1}, 1991–2005) in comparison to the two-core case (i.e., ~2 mm yr^{-1}).

Shallow subsidence (S_S) appears to be minimal in these low-permeability mineral-rich muds, as reported by Swales et al. (2015). This is because the subsidence rates for the RSETs are relative to the base of their benchmarks (i.e., S_D) and deep subsidence must influence the entire sediment column (i.e., recent ^{210}Pb SAR). The core-derived estimates of contemporary RSLR (i.e., 9.9, 9.3 mm yr^{-1}) that we largely attribute to subsidence are also an order of magnitude higher than the average ~0.35 mm yr^{-1} indicated by the vertical accumulation of at least 0.7 km of sediments during the Quaternary (Fig. 1).

In the present study, the PositioNZ GNSS network provides information on interseismic rates of land motion. Data from PositioNZ stations located in upper North Island, most of which were established in 2002–2005 (Auckland station [AUCK] established in 1995), indicate that this region is relatively stable during interseismic periods. In the immediate vicinity of the Hauraki Rift, data from the Coromandel PositioNZ station (CORM) indicates slow eastward movement relative to the AUCK station at ~1 mm yr^{-1} (Supplementary Information B). The 1.6 ± 0.5 mm yr^{-1} subsidence rate observed at the RSET-0 reference site, located on greywacke basement rock, is consistent with this apparent eastward tectonic extension. Vertical displacement of faults within the Hauraki Rift, in particular the Kerepehi Fault (Fig. 1), also occur during coseismic events and most recently approximately 1400 years ago (De Lange and Lowe, 1990). In the present study, campaign-GPS surveys of RSET benchmarks and the reference site, as well as RSLR inferred from ^{210}Pb profiles preserved in sediment cores, suggest that: (1) regional tectonic processes (i.e., ~1.6 mm yr^{-1}) may explain a small component of the subsidence trend in the mangrove forest; and (2) sediment compaction is the dominant process most of the time.

5.2. Conceptual sedimentary model of coastal wetlands unconstrained by sediment supply

The geomorphic evolution of the Firth mangrove forest since the 1950s has been reconstructed in detail by Swales et al. (2015). That study demonstrated that sedimentation is controlled by physical processes (in particular sediment supply, surface-elevation gain and resulting negative feedback with hydroperiod) rather than biophysical feedbacks following mangrove colonization. The geomorphic reconstruction also showed that the old-growth mangrove forest had aggraded to the upper limit of the tidal frame by the late 1960s. The present-day fringe forest only developed in the early-1990s, forming a vegetated barrier separated from the landward old-growth forest by a shallow tidal basin several-hundred metres wide. In fact, aggradation of the entire mangrove platform above MHWS tide level has only occurred in the last decade. Re-survey of the 2005 elevation profile seaward of RSET-2 (Fig. 3) in January 2013 indicates that the mangrove-forest platform had prograded seaward by approximately 30 m. Associated increases in surface elevation of ~30 mm yr^{-1} implied by these survey data are consistent with both recent ^{210}Pb SAR (25–31 mm yr^{-1}) and RSET (32–37 mm yr^{-1}, 2007–2014) measurements in the fringe forest (Swales et al., 2015). These observations suggest that the mangrove-forest sedimentary complex had recently switched from an aggradation- to progradation-dominated sedimentary regime.

The geomorphic development of the Firth mangrove forest can be considered within the framework of sequence stratigraphy, which is primarily derived from the concept of sediment accommodation space. Over geological time scales, the combination of sea-level fluctuations and subsidence combine, which results in cycles of sedimentation and erosion associated with changes in base level and accommodation space (Jervey, 1988; Posamentier et al., 1988; Schlager, 1993; Coe et al., 2002). On the shelf and onshore to intertidal settings, wave resuspension of sediments in particular also influences the available accommodation space by determining the local equilibrium profile or base level (Jervey, 1988; Walsh and Nittrouer, 2009). In the southern Firth, a 0.7 to 1 km thick sequence of unconsolidated sediments has accumulated during the Quaternary alone. This suggests that subsidence has been the dominant process controlling long-term relative sea level in this system. The mangrove-forest platform, presently near the upper limit of the tidal frame, represents a limiting case of marine accommodation space, with increases in the space available for sediment deposition being directly proportional to relative sea-level rise (Jervey, 1988). This proportional relationship between accommodation-space creation by sea-level rise and vertical land motion, and sedimentation has been termed a “keep-up” cycle by Soreghan and Dickinson (1994), with maximum accommodation preserved as aggradational facies in the sedimentary record.

Evidence preserved in coastal and estuarine sedimentary records has widely been used to reconstruct the chronology, magnitude and recurrence intervals of coseismic, interseismic and postseismic events and resulting changes in relative sea level during the Holocene (e.g., Ovenshine et al., 1976; Atwater, 1987; Nelson et al., 1996; Cochran et al., 2006; Dura et al., 2011; Shennan et al., 2014). These studies attribute subsidence inferred from estuarine and coastal wetland deposits largely to tectonic processes (i.e., earthquake ruptures, interseismic deformation) rather than sediment compaction. The results of the present study demonstrate that sediment compaction can be the dominant interseismic process even in tectonically active sedimentary basins, such as the Hauraki Rift.

Mangrove forests, once established, effectively reduce sediment resuspension through drag-induced dampening of tidal currents (Furukawa et al., 1997; Mazda and Wolanski, 2009) and wave attenuation (Massel et al., 1999; Alongi, 2008) caused by the mangrove-forest canopy and trunks and aboveground roots of individual trees (Spenceley, 1977; Woodroffe, 1992; Allison et al., 1995; Augustinus, 1995; Young and Harvey, 1996; Anthony and Gratiot, 2012). Thus, sediment resuspension is minimal in the old-growth forest and the creation of accommodation space and resulting sedimentation is ultimately constrained to RSLR (i.e., $RSLR_{sed} = S_T + RSLR_{tg}$). Similarly, the formation of shell ridges in estuaries transform high-energy wave-

dominated tidal flats into low-energy accreting intertidal-flats that ultimately aggrade to supratidal elevations at rates determined by RSLR (e.g., Heap and Nichol, 1997). The Firth of Thames mangrove forest has cycled through at least two aggradation and progradation cycles, ultimately controlled by the availability of accommodation space (Fig. 7).

In this mineral-sediment rich environment, the transition to a progradation mode occurs when the creation of new accommodation space in the mangrove-forest is limited to RSLR. Phases of rapid aggradation of the intertidal flat decades before and subsequent to mangrove-forest colonization since the 1960s (i.e., ^{210}Pb SAR 25–100 mm yr^{-1}) indicates that the long-term net onshore (wave-driven) fine-sediment flux substantially exceeds sediment accommodation space created by RSLR (Swales et al., 2015). Consequently, the sedimentation front shifts seaward and lower in the intertidal zone to the fringe forest and unvegetated tidal flats, where fine sediments can be accommodated despite more frequent wave resuspension.

5.3. Evaluating coastal wetland resilience — implications

Regional tide-gauge records are often used to evaluate the RSLR rate for coastal wetlands (Meckel, 2008; Webb et al., 2013). Cahoon (2014) proposed a method to estimate RSLR for a coastal wetland ($RSLR_{wet}$) being:

$$RSLR_{wet} = RSLR - VLM_w \quad (4)$$

where RSLR is the rate of relative sea level rise from a long-term tide gauge record (i.e., decades) and VLM_w is the surface-elevation trend relative to the RSET benchmark (i.e., does not account for deep subsidence). Thus, positive values of $RSLR_{wet}$ indicate submergence of the wetland whereas negative values of $RSLR_{wet}$ indicate wetland emergence as the rate of surface-elevation gain out-paces RSLR. This framework assumes that the RSLR measured at the tide gauge is representative of conditions in the coastal wetland. In fact, it is unlikely that tide-gauge records will be representative of the RSLR trend occurring in many coastal wetlands. This is due to differences in hydro-sedimentary setting and site-specific surface-elevation changes associated with biotic and abiotic wetland sedimentation processes (Cahoon, 2014). There are numerous examples in the literature where spatially-variable coastal-subsidence rates are the rule rather than the exception. This is the case in a range of environmental settings, including river deltas, tectonically active margins and in areas where human activities interrupt sediment supply or promote compaction from fluid extraction or where disturbances promote deposition (e.g., Cahoon et al., 2003; Carbognin et al., 2004; Peltier, 2004; Phien-wej et al., 2006; Meckel, 2008; Törnqvist et al., 2008; Syvitski et al., 2009; Doyle et al., 2010; Day et al., 2011; Kolker et al., 2011; Lang'at et al., 2014; Brown and Nicholls, 2015).

In the present study, the total subsidence rate measured at the Tararu tide gauge (3.6 ± 0.7 mm yr^{-1}) by the campaign-GPS surveys is significantly lower than at the RSET stations (7.7 ± 0.5 to 9.4 ± 0.3 mm yr^{-1}) located in the mangrove forest only ten kilometres distant. This may reflect to some degree the fact that the Tararu tide gauge is located in an adjacent sedimentary basin, bounded by the Kerepehi Fault (Fig. 1) that may have a differential subsidence rate. Regardless, our results demonstrate that evaluation of coastal wetland resilience to sea-level rise must be based on site-specific information because of the importance of local processes in determining the rate of RSLR.

An alternative approach to evaluate coastal-wetland resilience to sea-level rise, which explicitly accounts for spatially-variable RSLR, is to calculate the net rate of change in wetland elevation (ΔE_{wet}) as:

$$\Delta E_{wet} = RSET_{elev} - RSLR_{wet} \quad (5)$$

so that the site-specific elevation capital of a coastal wetland increases when $\Delta E_{wet} > 0$, where $RSET_{elev}$ is the measured substrate surface-elevation trend relative to the RSET benchmark (reduced to a vertical datum) and $RSLR_{wet}$ is the long-term RSLR trend for a coastal wetland. The value of $RSLR_{wet}$ is determined from: (1) suitable sedimentary records (i.e., SAR ∝ RSLR); and/or (2) total subsidence derived from campaign- or continuous-GPS measurements of benchmarks located within a coastal wetland, combined with RSLR estimated from a nearby tide gauge record adjusted for VLM (e.g., Watson et al., 2015). As we have demonstrated, radioisotope dating of sediment deposits can, under certain conditions, provide long-term estimates of RSLR in coastal wetlands.

6. Conclusions

The main objective of the present study was to evaluate if campaign-GPS measurements of RSET benchmarks, in combination with proxy measures of subsidence derived independently from sedimentary records, can be used to reliably estimate the contributions of subsidence associated with regional tectonic and local sedimentary processes to RSLR in a mature coastal wetland. A number of studies have utilised

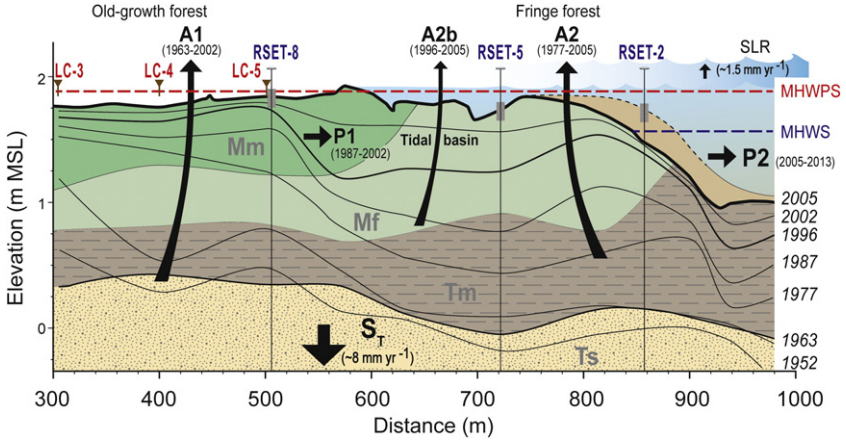

Fig. 7. Conceptual sedimentary model of the tidal flat/mangrove forest complex, Firth of Thames, showing cycles of aggradation (A) and progradation (P) driven by the creation and infilling of accommodation space by sea-level rise (SLR), total subsidence (S_T) and mineral sediment supply. Sediment accumulation rates are ultimately limited to relative sea-level rise (i.e., RSLR = S_T + SLR), when surface elevation reaches the upper limit of the tidal frame, above Mean High Water Spring (MHWS) tide level. Sediment core sites: LC-3 to LC-5. Rod Surface Elevation Table benchmarks: RSET-2, -5 and -8. Sedimentary facies: laminated to bedded muddy sands (Ts); partially-bioturbated muds with rare silt laminae (Tm); bioturbated muds with mangrove roots (Mf); and nodular-bioturbated muds with abundant mangrove roots and precipitates (Mm). Isochrones: substrate surface elevations (1952–2005) reconstructed from radioisotope dating of cores and RSET data. Reproduced and modified from Swales et al. (2015).

the accommodation space concept to estimate RSLR from salt marsh sedimentary records (e.g., Gehrels et al., 2002, 2008; Donnelly et al., 2004; Fadil et al., 2013). The present study is the first, as far as we are aware, to combine sedimentary records with direct measurements of vertical land motion at RSET stations located within a coastal wetland.

Globally, RSET networks have been established at hundreds of sites and are being used to determine, among other things, the resilience of salt marshes and mangrove forests in temperate and tropical settings to sea-level rise (Webb et al., 2013; Cahoon, 2014; Lovelock et al., 2015b). The findings of the present study demonstrate firstly that the vertical stability of RSET benchmarks should not be assumed, particularly in tectonically-active settings, deltas and sedimentary basins, where some of the world's largest mangrove forests occur (Giri et al., 2011). Secondly, tide-gauge records in many cases may not provide reliable estimates of RSLR within a coastal wetland. Lastly, campaign-GPS measurements of RSET in combination with sedimentary records in some environmental settings can be used to: (1) quantify RSLR and total subsidence rates over decadal time scales; and (2) evaluate the relative contributions of regional-scale deep subsidence and local-scale shallow subsidence associated with compaction of recent deposits.

Acknowledgements

We thank Ken Krauss (USGS National Wetland Research Centre) and Sam Bentley (Department of Geology and Geophysics, Louisiana State University) and the anonymous reviewers for their constructive comments on the manuscript. Don Cahoon (USGS) generously assisted with the installation of the RSET benchmarks and Mark Smith (NIWA) provided logistical support. The contributions of Doug Stewart (Science and Strategy Directorate, Waikato Regional Council), Cliff Hart & Ron Ovenden (NIWA), who assisted with the campaign-GPS surveys are greatly appreciated. Mike Allis (NIWA) provided guidance on the geotechnical evaluation of the RSET benchmark stability and sea-level data was provided by Rob Bell (NIWA). Max Oulton (University of Waikato, NZ) drafted Figs. 1, 3–4 and 7. Radioisotope analyses were conducted by the ESR National Centre for Radiation Science, Christchurch, New Zealand. This study was supported by the NZ Ministry of Business, Innovation and Employment (CO1X0307), Waikato Regional Council and NIWA Core Funding (FWCE1507, FWCE1607). Fig. 1b was reproduced from Hochstein, M.P. and Nixon, I.M. (1979). Geophysical study of the Hauraki Depression, North Island, New Zealand. New Zealand Journal of Geology and Geophysics 22(1): 1–19, copyright© The Royal Society of New Zealand, reprinted by permission of Taylor and Francis Ltd., www.tandfonline.com on behalf of The Royal Society of New Zealand. Fig 7 was reproduced and modified from Swales A., Bentley, S.J. and Lovelock C.E., Earth Surf. Process Landf. 40, 2015, 1672–1687 with permission. Copyright © 2015 John Wiley & Sons, Ltd. Aerial photography of the southern Firth of Thames provided by Waikato Regional Council from various sources and Terralink International (WRAPS 2013).

In memory of Vernon Pickett, PhD, surveyor, scientist and friend (18 January 1951–7 May 2014).

Map 1. KML file containing the Google maps of the most important areas describe in this article.

Map 2. KML file containing the Google maps of the most important areas describe in this article.

Appendix A. Supplementary data

Supplementary data associated with this article can be found in the online version, at doi:http://dx.doi.org/10.1016/j.margeo.2016.04.015. This data include the Google map of the most important areas described in this article.

References

Allison, M.A., Nittrouer, C.A., Faria Jr., L.E.C., 1995. Rates and mechanisms of shoreface progradation and retreat downdrift of the Amazon River mouth. Mar. Geol. 125, 373–392.

Alongi, D.M., 2008. Mangrove forests: resilience, protection from tsunamis, and responses to global climate change. Estuar. Coast. Shelf Sci. 76, 1–13.

Altamimi, Z., Métivier, L., Collilieux, X., 2012. ITRF2008 plate motion model. J. Geophys. Res. 117, B07402. http://dx.doi.org/10.1029/2011JB008930.

Anthony, E.J., Gratiot, N., 2012. Coastal engineering and large-scale mangrove destruction in Guyana, South America: averting an environmental catastrophe in the making. Ecol. Eng. 47, 268–273.

Atwater, B.F., 1987. Evidence for great earthquakes along the outer coast of Washington state. Science 236, 942–944. http://dx.doi.org/10.1126/science.236.4804.942.

Augustinus, P.G.E.F., 1995. Geomorphology and sedimentology of mangroves. In: Perillo, G.M.E. (Ed.), Developments in Sedimentology 53. Geomorphology and sedimentology of estuaries. Elsevier Science, Amsterdam, pp. 333–357.

Beavan, J., 2005. Noise properties of continuous GPS data from concrete pillar geodetic monuments in New Zealand and comparison with data from U.S. deep drilled braced monuments. J. Geophys. Res. Solid Earth 110, B08410. http://dx.doi.org/10.1029/2005JB003642.

Beavan, J., Denys, P., Denham, M., Hager, B., Herring, T., Molnar, P., 2010. Distribution of present-day vertical deformation across the Southern Alps, New Zealand, from 10 years of GPS data. Geophys. Res. Lett. 37 (16), L16305. http://dx.doi.org/10.1029/2010gl044165.

Beavan, J., Wallace, L., Palmer, N., Denys, P., Ellis, S., Fournier, N., Hreinsdottir, S., Pearson, C., Denham, M., 2016. New Zealand GPS velocity field: 1995–2013. N. Z. J. Geol. Geophys. http://dx.doi.org/10.1080/00288306.2015.1112817.

Bird, E.C.F., 1986. Mangroves and intertidal morphology in Westernport Bay, Victoria, Australia. Mar. Geol. 69, 251–271.

Blewitt, G., Lavallée, D., 2002. Effect of annual signals on geodetic velocity. J. Geophys. Res. Solid Earth 107 (B7). http://dx.doi.org/10.1029/2001jb000570 (ETG 9-1–ETG 9-11).

Boumans, R., Day, J.W., 1993. High precision measurements of sediment elevation in shallow coastal areas using a sedimentation-erosion table. Estuaries 16, 375–380.

Brown, S., Nicholls, R.J., 2015. Subsidence and human influences in mega deltas: the case of the Ganges–Brahmaputra–Meghna. Sci. Total Environ. 527–528, 362–374.

Cahoon, D.R., 2006. A review of major storm impacts on coastal wetland elevations. Estuar. Coasts 29 (6 A), 889–898.

Cahoon, D.R., 2014. Estimating relative sea-level rise and submergence potential at a coastal wetland. Estuar. Coasts 38 (3), 1077–1084. http://dx.doi.org/10.1007/s12237-014-9872-8.

Cahoon, D.R., Reed, D.R., Day, J.W., 1995. Estimating shallow subsidence in microtidal salt marshes of the southeastern United States: Kaye and Barghoorn revisited. Mar. Geol. 128, 1–9.

Cahoon, D.R., Day, J.W., Reed, D.J., 1999. The influence of surface and shallow subsurface soil processes on wetland elevation: a synthesis. Current Topics in Wetland Biogeochemistry. 3, pp. 72–88.

Cahoon, D.R., Lynch, J.C., Perez, B.C., Segura, B., Holland, R.D., Stelly, C., Stephenson, G., Hensel, P., 2002. High-precision measurements of wetland sediment elevation: II. The Rod Surface Elevation Table. J. Sediment. Res. 72 (5), 734–739.

Cahoon, D.R., Hensel, P.F., Rybczyk, J., McKee, K.L., Proffitt, C.E., Perez, B.C., 2003. Mass tree mortality leads to mangrove peat collapse at Bay Islands, Honduras after Hurricane Mitch. J. Ecol. 91 (6), 1093–1105.

Cahoon, D.R., Hensel, P.F., Spencer, T., Reed, D.J., McKee, K.L., Saintilan, N., 2006. Coastal wetland vulnerability to relative sea-level rise: wetland elevation trends and process controls. In: Verhoeven, J.T.A., et al. (Eds.), Wetlands and Natural Resource Management. Springer-Verlag, Berlin, pp. 271–292.

Cahoon, D.R., Guntenspergen, G.R., 2010. Climate change, sea-level rise and coastal wetlands. National Wetlands Newsl. 2010, 8–12 (Jan–Feb).

Carbognin, L., Teatini, P., Tosi, L., 2004. Eustacy and land subsidence in the Venice lagoon at the beginning of the new millennium. J. Mar. Syst. 51, 345–353.

Carminati, E., Martinelli, G., 2002. Subsidence rates in the Po Plain, Northern Italy: the relative impact of natural and anthropogenic causation. Eng. Geol. 66, 241–255.

Cazenave, A., Llovel, W., 2010. Contemporary sea level rise. Ann. Rev. Mar. Sci. 2, 145–173. http://dx.doi.org/10.1146/annurev-marine-120308-081105.

Cenni, N., Viti, M., Baldi, P., Mantovani, E., Bacchetti, M., Vannucchi, A., 2013. Present vertical movements in Central and Northern Italy from GPS data: possible role of natural and anthropogenic causes. J. Geodyn. 71, 74–85. http://dx.doi.org/10.1016/j.jog.2013.07.004.

Chick, L.M., De Lange, W.P., Healy, T.R., 2001. Potential tsunami hazard associated with the Kerepehi Fault, Firth of Thames, New Zealand. Nat. Hazards 24, 309–318.

Church, J.A., White, N.J., 2011. Sea-level rise from the late 19th to the early 21st Century. Surv. Geophys. 32, 585–602. http://dx.doi.org/10.1007/s10712-011-9119-1.

Clarke, L.D., Hannon, N.J., 1970. The mangrove swamp and salt marsh communities of the Sydney district. III. Plant growth in relation to salinity and waterlogging. J. Ecol. 58, 351–369.

Cochran, U., Berryman, K., Zachariasen, J., Mildenhall, D., Haywood, B., Southall, K., Hollis, C., Barker, P., Wallace, L., Alloway, B., Wilson, K., 2006. Paleoecological insights into subduction zone earthquake occurrence, eastern North Island, New Zealand. Geol. Soc. Am. Bull. 118 (9/10), 1051–1074.

Coe, A., Bosence, D., Church, K., Flint, S., Howell, J., Wilson, C., 2002. The Sedimentary Record of Sea Level Change. Cambridge University Press 288 pp.

Curran, M., Cole, M., Allaway, W.G., 1986. Root aeration and respiration in young mangrove plants (*Avicennia marina* (Forsk.) Vierh.). J. Exp. Bot. 37, 1225–1233.

Dach, R., Lutz, S., Walser, P., Fridez, P., 2015. Bernese GNSS Software Version 5.2. Astronomical Institute, University of Bern, Bern, Switzerland (851 pp.).

Day, J.W., Kemp, G.P., Reed, D.J., Cahoon, D.R., Boumans, R.M., Suhayda, J.M., Gambrell, R., 2011. Vegetation death and rapid loss of surface elevation in two contrasting

Mississippi delta salt marshes: the role of sedimentation, autocompaction and sea-level rise. Ecol. Eng. 37, 229–240.
De Lange, P.J., Lowe, D.J., 1990. History of vertical displacement of Kerepehi Fault at Kopouatai bog, Hauraki lowlands, New Zealand, since c. 10,700 years ago. N. Z. J. Geol. Geophys. 33, 277–283.
Donnelly, J.P., Cleary, P., Newby, P., Ettinger, R., 2004. Coupling of instrumental and geological records of sea-level change. Evidence from southern New England of an increase in the rate of sea-level rise in the late 19th century. Geophys. Res. Lett. 31, L05203. http://dx.doi.org/10.1029/2003GL018933.
Doyle, T.W., Krauss, K.W., Conner, W.H., From, A.S., 2010. Predicting the retreat and migration of tidal forests along the northern Gulf of Mexico under sea-level rise. For. Ecol. Manag. 259 (4), 770–777.
Dura, T., Rubin, C.M., Kelsey, H.M., Horton, B.P., Hawkes, A., Vane, C.H., Daryono, M., Pre, C.G., Ladinsky, T., Bradley, S., 2011. Stratigraphic record of Holocene coseismic subsidence, Padang, West Sumatra. J. Geophys. Res. 116, B11306. http://dx.doi.org/10.1029/2011JB008205.
Edwards, S.J., Clarke, P.J., Penna, N.T., Goebell, S., 2010. An examination of network RTK GPS services in Great Britain. Surv. Rev. 42 (316), 107–121.
Ellison, J.C., 1993. Mangrove retreat with rising sea-level, Bermuda. Estuar. Coast. Shelf Sci. 37, 75–87.
Ellison, J.C., 2008. Long-term retrospection on mangrove development using sediment cores and pollen analysis: a review. Aquat. Bot. 89, 93–104.
Fadil, A., Denys, P., Tenzer, R., Grenfell, H.R., Willis, P., 2013. New Zealand 20th century sea level rise: resolving the vertical land motion using space geodetic and geological data. J. Geophys. Res. Oceans 118, 6076–6091.
Firuzabadi, D., King, R., 2012. GPS precision as a function of session duration and reference frame using multi-point software. GPS Solutions 16 (2), 191–196.
Furukawa, K., Wolanski, E., Mueller, H., 1997. Currents and sediment transport in mangrove forests. Estuar. Coast. Shelf Sci. 44, 301–310.
Galloway, R.W., 1982. Distribution and physiographic patterns of Australian mangroves. In: Clough, B.F. (Ed.), Mangrove Ecosystems in Australia: Structure, Function and Management. Australian Institute of Marine Science, Townsville, Australia, pp. 31–54.
Gehrels, W.R., Belknap, D.F., Black, S., Newnham, R.M., 2002. Rapid sea-level rise in the Gulf of Maine, USA since AD 1800. The Holocene 12, 383–389.
Gehrels, W.R., Hayward, B.W., Newnham, R.M., Southall, K.E., 2008. A 20th century acceleration of sea-level rise in New Zealand. Geophys. Res. Lett. 35, L02717. http://dx.doi.org/10.1029/2007GL032632.
Giri, C., Ochieng, E., Tieszen, L.L., Zhu, Z., Singh, A., Loveland, T., Maesk, J., Duke, N., 2011. Status and distribution of mangrove forests of the world using earth observation satellite data. Glob. Ecol. Biogeogr. 20, 154–159.
Hackl, M., Malservisi, R., Hugentobler, U., Wonnacott, R., 2011. Estimation of velocity uncertainties from GPS time series: examples from the analysis of the South African TrigNet network. J. Geophys. Res. Solid Earth 116 (B11), B11404. http://dx.doi.org/10.1029/2010jb008142.
Häkli, P., Koivula, H., Puupponen, J., 2008. Assessment of Practical 3-D Geodetic Accuracy for Static GPS Surveying, FIG Working Week 2008, Stockholm, Sweden 14–19 June 2008. (Source: https://www.fig.net/resources/proceedings/fig_proceedings/fig2008/papers/ts03h/ts03h_01_hakli_etal_2994.pdf).
Hannah, J., Bell, R.G., 2012. Regional sea level trends in New Zealand. J. Geophys. Res. 117, C01004. http://dx.doi.org/10.1029/2011JC007591.
Healy, T., 2002. Muddy coasts of mid-latitude oceanic islands on an active plate margin — New Zealand. In: Healy, T., Wang, Y., Healy, J.-A. (Eds.), Muddy Coasts of the World: Processes, Deposits and Function, pp. 347–374.
Heap, A., Nichol, S.L., 1997. The influence of limited accommodation space on the stratigraphy of an incised-valley succession: Weiti River estuary, New Zealand. Mar. Geol. 144, 229–252.
Hicks, D.M., Shankar, U., McKerchar, A.I., Basher, L., Jessen, M., Lynn, I., Page, M., 2011. Suspended sediment yields from New Zealand Rivers. J. Hydrol. (NZ) 50 (1), 81–142.
Hochstein, M.P., Nixon, I.M., 1979. Geophysical study of the Hauraki Depression, North Island, New Zealand. N. Z. J. Geol. Geophys. 22, 1–19.
Hochstein, M.P., Tearney, K., Rawson, S., Davey, F.J., Davidge, S., Henreys, S., Backshal, D., 1986. Structure of the Hauraki Rift (New Zealand). Bull. Roy. Soc. NZ 24, 333–348.
Hofmann-Wellenhof, B., Lichtenegger, H., Collins, J., 2001. Global Positioning System: Theory and Practice. fifth ed. Springer-Verlag, Wien.
Hovenden, M.J., Curran, M., Cole, M.A., Goulter, P.F.E., Skelton, N.J., Allaway, W.G., 1995. Ventilation and respiration in roots of one-year-old seedlings of grey mangrove *Avicennia marina* (Forsk.) Vierh. Hydrobiologia 295, 23–29.
IPCC. 2013: Climate Change. 2013. The Physical Science Basis. Contribution of Working Group I to the Fifth Assessment Report of the Intergovernmental Panel on Climate Change [Stocker, TF, Qin D, Plattner, G-K, Tignor M, Allen, SK, Boschung J, Nauels, A, Xia, Y, Bex, V, Midgley, PM. (Eds.)]. Cambridge University Press, Cambridge, United Kingdom and New York, NY, USA, (1535 pp.)
Jervey, M.T., 1988. Quantitative geological modelling of siliciclastic rock sequences and their seismic expressions. In: Wilgus, C.K., Hastings, B.S., Kendall, C.G.S.C., Posamentier, H.W., Ross, C.A., Van Wagoner, J.C. (Eds.), Sea Level Changes: An Integrated Approach. Society of Economic Palaeontologists and Mineralogists Special Publication 42, pp. 47–69.
Joint Committee for Guides in Metrology (JCGM), 2008. Evaluation of measurement data — guide to the expression of uncertainty in measurement, Report JCGM 100: 2008. Working Group 1 of the Joint Committee for Guides in Metrology. Sèvres, BIPM (134 pp.).
Kaye, C.A., Barghoorn, E.S., 1964. Late Quaternary sea-level change and crustal rise at Boston Massachusetts, with notes on the autocompaction of peat. Geol. Soc. Am. Bull. 75, 63–80.
Kearns, T.J., Wang, G.M., Bao, Y., Jiang, J., Lee, D., 2015. Current land subsidence and groundwater level changes in the Houston metropolitan area (2005–2012). J. Surv. Eng. 141 (4). http://dx.doi.org/10.1061/(ASCE)SU.1943-5428.0000147.
Krishnaswami, S., Benninger, L.K., Aller, R.C., Von Damm, K.L., 1980. Atmospherically-derived radionuclides as tracers of sediment mixing and accumulation in near-shore marine and lake sediments: evidence from Be-7, Pb-210, and Pu-239, 240. Earth Planet. Sci. Lett. 47, 307–318.
Kolker, A.S., Allison, M.A., Hameed, S., 2011. An evaluation of subsidence rates and sea-level variability in the northern Gulf of Mexico. Geophys. Res. Lett. 38, L21404. http://dx.doi.org/10.1029/2011GL049458.
Krauss, K., Allen, J.A., Cahoon, D.R., 2003. Differential rates of vertical accretion and elevation change among aerial root types in Micronesian mangrove forests. Estuar. Coast. Shelf Sci. 56, 251–259.
Krauss, K.W., McKee, K.L., Lovelock, C.E., Cahoon, D.R., Saintilan, N., Reef, R., Chen, L., 2013. How mangroves adjust to rising sea level. New Phytol. http://dx.doi.org/10.1111/nph.12605.
Lang'at, J.K.S., Kairo, J.G., Mencuccini, M., Bouillon, S., Skov, M.W., Waldrom, S., Huxham, M., 2014. Rapid losses of surface elevation following tree girdling and cutting in tropical mangroves. PLoS One 9 (9), e107868. http://dx.doi.org/10.1371/journal.pone.0107868.
Lovelock, C.E., Bennion, V., Grinham, A., Cahoon, D.R., 2011. The role of surface and subsurface processes in keeping pace with sea level rise in intertidal wetlands of Moreton Bay, Queensland, Australia. Ecosystems 14 (5), 745–757.
Lovelock, C.E., Cahoon, D.R., Friess, D.A., Guntenspergen, G.R., Krauss, K.W., Reef, R., Rogers, K., Saunders, M., Sidik, F., Swales, A., Saintilan, N., Thuyen, L.X., Triet, T., 2015b. The vulnerability of Indo-Pacific mangrove forests to sea level rise. Nature 526, 559–563. http://dx.doi.org/10.1038/nature15538.
Mao, A., Harrison, C.G.A., Dixon, T.H., 1999. Noise in GPS coordinate time series. J. Geophys. Res. 104 (B2), 2797–2816.
Massel, S.R., Furukawa, K., Brinkman, R.M., 1999. Surface wave propagation in mangrove forests. Fluid Dyn. Res. 24, 219–249.
Matthews, K.M., 1989. Radioactive fallout in the South Pacific — a history. Part 1. Deposition in New Zealand. Report NRL 1989/2. National Radiation Laboratory, Christchurch, New Zealand.
Mazda, Y., Wolanski, E., 2009. Hydrodynamics and modelling of water flow in mangrove areas. In: G.M.E., P., et al. (Eds.), Coastal Wetlands—An Integrated Ecosystem Approach. Elsevier, Amsterdam, pp. 231–261.
Meckel, T.A., 2008. An attempt to reconcile subsidence rates determined from various techniques in southern Louisiana. Quat. Sci. Rev. 27, 1517–1522.
McKee, K.L., Cahoon, D.R., Feller, I.C., 2007. Caribbean mangroves adjust to rising sea level through biotic controls on change in soil elevation. Glob. Ecol. Biogeogr. 16, 545–556.
McKee, K.L., 2011. Biophysical controls on accretion and elevation change in Caribbean mangrove ecosystems. Estuar. Coast. Shelf Sci. 91, 475–483.
Morrisey, D.J., Swales, A., Dittmann, S., Morrison, M.A., Lovelock, C.E., Beard, C.M., 2010. The ecology and management of temperate mangroves. Oceanography and Marine Ecology: An Annual Review. 48, pp. 43–160.
Nelson, A.R., Shennan, I., Long, A.J., 1996. Identifying coseismic subsidence in tidal-wetland stratigraphic sequences at the Cascadia subduction zone of western North America. J. Geophys. Res. 101, 6115–6135. http://dx.doi.org/10.1029/ 95JB01051.
Nerem, R.S., van Dam, T.M., Schenewerk, M.S., 1998. Chesapeake Bay subsidence monitored as wetlands loss continues. EOS Trans. 79, 149–157.
Nittrouer, C.A., Sternberg, R.W., 1981. The formation of sedimentary strata in an allochthonous shelf environment: the Washington continental shelf. Mar. Geol. 42, 201–232.
Ovenshine, A.T., Lawson, D.E., Bartsch-Winkler, S.R., 1976. The Placer River silt — an intertidal deposit caused by the 1964 Alaska earthquake. J. Res. U. S. Geol. Surv. 4 (2), 151–162.
Pearson, C., Crook, C., Jordan, A., Denys, P., 2015. PositioNZ-PP: An Online GPS Processing Application for New Zealand. Springer, Berlin Heidelberg, pp. 1–7.
Peltier, W.R., 2004. Global glacial isostasy and the surface of the ice-age earth: the ICE-5G (VM2) model and GRACE. Annu. Rev. Earth Planet. Sci. 32, 111–149.
Phien-wej, N., Giao, P.H., Nutalaya, P., 2006. Land subsidence in Bangkok, Thailand. Eng. Geol. 82, 187–201.
Pillans, B., 1986. A late Quaternary uplift map for North Island, New Zealand. Bull. Roy. Soc. NZ 24, 409–417.
Posamentier, H.W., Jervey, M.T., Vail, P.R., 1988. Eustatic controls on clastic deposition I — conceptual framework. In: Wilgus, C.K., Hastings, B.S., Kendall, C.G.S.C., Posamentier, H.W., Ross, C.A., Van Wagoner, J.C. (Eds.), Sea Level Changes: An Integrated Approach. SEPM Spec. Publ. Vol. 42, pp. 110–124.
Reed, D.J., 2002. Sea-level rise and coastal marsh sustainability: geological and ecological factors in the Mississippi delta plain. Geomorphology 48, 233–243.
Rogers, K., Saintilan, N., Heijnis, H., 2005. Mangrove encroachment of salt marsh in Western Port Bay, Victoria: the role of sedimentation, subsidence, and sea level rise. Estuaries 28 (4), 551–559.
Rogers, K., Saintilan, N., Howe, A.J., Rodríguez, J.F., 2013. Sedimentation, elevation and marsh evolution in a southeastern Australian estuary during changing climatic conditions. Estuar. Coast. Shelf Sci. 133, 172–181.
Santamaría-Gómez, A., Gravelle, M., Collilieux, X., Guichard, M., Martín-Míguez, B., Tiphaneau, P., Wöppelmann, G., 2012. Mitigating the effects of vertical land motion in tide gauge records using a state-of-the-art GPS velocity field. Glob. Planet. Chang. 98–99, 6–17. http://dx.doi.org/10.1016/j.gloplacha.2012.07.007.
Schlager, W., 1993. Accommodation and supply — a dual control on stratigraphic sequences. Sediment. Geol. 86, 111–136.
Shennan, I., Bruhn, R., Barlow, N., Good, K., Hocking, E., 2014. Late Holocene great earthquakes in the eastern part of the Aleutian megathrust. Quat. Sci. Rev. 84, 86–97.
Slangen, A.B.A., van de Wal, R.S.W., Wada, Y., Vermeersen, L.L.A., 2014. Comparing tide gauge observations to regional patterns of sea-level change. Earth Syst. Dyn. 5, 243–255.

Soler, T., Michalak, P., Weston, N.D., Snay, R.A., Foote, R.H., 2006. Accuracy of OPUS solution for 1- to 4-h observing sessions. GPS Solutions 10, 45–55.
Soreghan, G.S., Dickinson, W.R., 1994. Generic types of stratigraphic cycles controlled by eustacy. Geology 22, 759–761.
Spenceley, A.P., 1977. The role of pneumatophores in sedimentary processes. Mar. Geol. 24, M31–M37.
Swales, A., Bentley, S.J., Lovelock, C., 2015. Mangrove-forest evolution in a sediment-rich estuarine system: opportunists or agents of geomorphic change? Earth Surf. Process. Landf. 40, 1672–1687. http://dx.doi.org/10.1002/esp.3759.
Syvitski, J.P.M., Vorosmarty, C.J., Kettner, A.J., Green, P., 2005. Impact of humans on the flux of terrestrial sediment to the global coastal ocean. Science 308, 376–380.
Syvitski, J.P.M., Kettner, A.J., Overeem, I., Hutton, E.W.H., Hannon, M.T., Brakenridge, G.R., Day, J., Vorosmarty, C.J., Saito, Y., Giosan, L., Nicholls, R.J., 2009. Sinking deltas due to human activities. Nat. Geosci. 2, 681–686.
Törnqvist, T.E., Wallace, D.J., Storms, J.E.A., Wallinga, J., Van Dam, R.L., Blaauw, M., Derksen, M.S., Klerks, C.J.W., Meijnenken, C., Snijders, E.M.A., 2008. Mississipi Delta subsidence primarily caused by compaction of Holocene strata. Nat. Geosci. 1 http://dx.doi.org/10.1038/ngeo129.
Walling, D.E., 1999. Linking land use, erosion and sediment yields in river basins. Hydrobiologia 410, 223–240.
Wallace, L.M., Beavan, J., McCaffrey, R., Darby, D., 2004. Subduction zone coupling and tectonic block rotations in the North Island, New Zealand. J. Geophys. Res. Solid Earth 109, B12406. http://dx.doi.org/10.1029/2004JB003241.
Walsh, J.P., Nittrouer, C.A., 2009. Understanding fine-grained river-sediment dispersal on continental margins. Mar. Geol. 263, 34–45.
Watson, C.S., White, N.J., Church, J.A., King, M.A., Burgette, R.J., Legresy, B., 2015. Unabated global mean sea level rise over the satellite altimeter era. Nat. Clim. Chang. 5, 565–569.
Wang, G., Yu, J., Ortega, J., Saenz, G., Burrough, T., Neill, R., 2013. A stable reference frame for the study of ground deformation in the Houston metropolitan area, Texas. J. Geogr. Sci. 3 (3). http://dx.doi.org/10.2478/jogs-2013-0021.
Webb, E.L., Friess, D.A., Krauss, K.W., Cahoon, D.R., Guntenspergen, G.R., Phelps, J., 2013. A global standard for monitoring coastal wetland vulnerability to accelerated sea-level rise. Nat. Clim. Chang. 3, 458–465.
Weston, N.B., 2014. Declining sediments and rising seas: an unfortunate convergence for tidal wetlands. Estuar. Coasts 37, 1–23.
Williams, S.D.P., Bock, Y., Fang, P., Jamason, P., Nikolaidis, R.M., Prawirodirdjo, L., Miller, M., Johnson, D.J., 2004. Error analysis of continuous GPS position time series. J. Geophys. Res. Solid Earth 109 (B3), B03412. http://dx.doi.org/10.1029/2003jb002741.
Woodroffe, C.D., 1992. Mangrove sediments and geomorphology. In: Robertson, A.I., Alongi, D.M. (Eds.), Tropical Mangrove Ecosystems. American Geophysical Union, Washington DC, pp. 7–41.
Woodroffe, C.D., Davies, G., 2009. The morphology and development of tropical coastal wetlands. In: Perillo, G.M.E., et al. (Eds.), Coastal Wetlands — An Integrated Ecosystem Approach. Elsevier, Amsterdam, pp. 65–88.
Wöppelmann, G., Marcos, M., Santamaría-Gómez, A., Martín-Míguez, B., Bouin, M.N., Gravelle, M., 2014. Evidence for a differential sea level rise between hemispheres over the twentieth century. Geophys. Res. Lett. 41, 1639–1643. http://dx.doi.org/10.1002/2013gl059039.
Young, B.M., Harvey, L.E., 1996. A spatial analysis of the relationship between mangrove (*Avicennia marina* var. australasica) physiognomy and sediment accretion in the Hauraki Plains, New Zealand. Estuar. Coast. Shelf Sci. 42, 231–246.

Further-reading

Lovelock, C.E., Adame, M.F., Bennion, V., Hayes, M., Reef, R., Santini, N., Cahoon, D.R., 2015a. Sea level and turbidity controls on mangrove soil surface elevation change. Estuar. Coast. Shelf Sci. 153, 1–9.